

53BP1 Mediates Productive and Mutagenic DNA Repair through Distinct Phosphoprotein Interactions

Elsa Callen,¹ Michela Di Virgilio,³ Michael J. Kruhlak,² Maria Nieto-Soler,⁴ Nancy Wong,¹ Hua-Tang Chen,¹ Robert B. Faryabi,¹ Federica Polato,¹ Margarida Santos,¹ Linda M. Starnes,⁵ Duane R. Wesemann,⁶ Ji-Eun Lee,⁷ Anthony Tubbs,⁸ Barry P. Sleckman,⁸ Jeremy A. Daniel,⁵ Kai Ge,⁷ Frederick W. Alt,⁶ Oscar Fernandez-Capetillo,⁴ Michel C. Nussenzweig,³ and André Nussenzweig^{1,*}

¹Laboratory of Genome Integrity

²Experimental Immunology Branch

National Cancer Institute, NIH, Bethesda, MD 20892, USA

³Laboratory of Molecular Immunology and Howard Hughes Medical Institute, Rockefeller University, New York, NY 10065, USA

⁴Genomic Instability Group, Spanish National Cancer Research Centre (CNIO), Madrid 28029, Spain

⁵The Novo Nordisk Foundation Center for Protein Research, Faculty of Health and Medical Sciences, University of Copenhagen, Copenhagen, Denmark

⁶Program in Cellular and Molecular Medicine, Immune Disease Institute and Howard Hughes Medical Institute, Children's Hospital, Boston, MA 02115, USA

⁷Laboratory of Endocrinology and Receptor Biology, National Institute of Diabetes and Digestive and Kidney Diseases, NIH, Bethesda, MD 20892, USA

⁸Department of Pathology and Immunology, Washington University School of Medicine, St. Louis, MO 63110, USA

*Correspondence: andre_nussenzweig@nih.gov

<http://dx.doi.org/10.1016/j.cell.2013.05.023>

SUMMARY

The DNA damage response (DDR) protein 53BP1 protects DNA ends from excessive resection in G1, and thereby favors repair by nonhomologous end-joining (NHEJ) as opposed to homologous recombination (HR). During S phase, BRCA1 antagonizes 53BP1 to promote HR. The pro-NHEJ and antirecombinase functions of 53BP1 are mediated in part by RIF1, the only known factor that requires 53BP1 phosphorylation for its recruitment to double-strand breaks (DSBs). Here, we show that a 53BP1 phosphomutant, 53BP1^{8A}, comprising alanine substitutions of the eight most N-terminal S/TQ phosphorylation sites, mimics 53BP1 deficiency by restoring genome stability in BRCA1-deficient cells yet behaves like wild-type 53BP1 with respect to immunoglobulin class switch recombination (CSR). 53BP1^{8A} recruits RIF1 but fails to recruit the DDR protein PTIP to DSBs, and disruption of PTIP phenocopies 53BP1^{8A}. We conclude that 53BP1 promotes productive CSR and suppresses mutagenic DNA repair through distinct phosphodependent interactions with RIF1 and PTIP.

INTRODUCTION

Class switch recombination (CSR) is initiated by activation-induced cytidine deaminase (AID), which generates multiple

double-strand breaks (DSBs) at highly repetitive immunoglobulin (Ig) switch regions. Paired distal DSBs are then rejoined by nonhomologous end-joining (NHEJ), thereby replacing Igμ by a downstream constant region (Igγ, Igε, or Igα). Alternatively, if DSBs persist, a homology-driven pathway that involves resection of repetitive switch regions, can repair DSBs locally. Such abortive “intraswitch” recombination events are increased at the expense of CSR in the absence of 53BP1 (Reina-San-Martin et al., 2007), a key suppressor of end resection (Bothmer et al., 2010; Bouwman et al., 2010; Bunting et al., 2010; Cao et al., 2009; Difilippantonio et al., 2008).

In addition to its productive effect on CSR, 53BP1 blocks DNA ends from resection in BRCA1-deficient cells, leading to toxic radial chromosomes that arise from NHEJ (Bouwman et al., 2010; Bunting et al., 2010, 2012; Cao et al., 2009). Deletion of 53BP1 leads to deposition of homologous recombination (HR) factors RPA and RAD51 on single-strand DNA, which, in the case of recombining switch regions, promotes intraswitch recombination (Yamane et al., 2013) and, in the setting of BRCA1 deficiency, restores HR (Bouwman et al., 2010; Bunting et al., 2010; Cao et al., 2009). Thus, DNA end protection by 53BP1 is critical for CSR in G1 but can unleash genome instability in S phase.

In addition to DNA end-blocking activities that disfavor HR and thereby promote NHEJ, 53BP1 has been suggested to directly mediate long-range chromosomal interactions and DSB mobility that facilitates the juxtaposition of distal DNA ends. These activities are believed to be responsible for 53BP1’s ability to support recombination of DSB ends that are far apart during V(D)J recombination and class switch recombination (Callén et al., 2007b; Difilippantonio et al., 2008) and to fuse uncapped telomeric DNA ends (Dimitrova et al., 2008). Both pro-NHEJ and

anti-HR functions require the direct physical association of 53BP1 with DNA ends but also necessitate the DSB-induced phosphorylation of its N-terminal ATM/ATR kinase sites (Bothmer et al., 2011; Ward et al., 2006).

The DNA damage response (DDR) protein RIF1 was recently identified as an essential factor recruited by phosphorylated 53BP1 to promote NHEJ and block HR (Chapman et al., 2013; Di Virgilio et al., 2013; Escribano-Díaz et al., 2013; Feng et al., 2013; Zimmermann et al., 2013). Like 53BP1, RIF1 is required for CSR (Chapman et al., 2013; Di Virgilio et al., 2013; Escribano-Díaz et al., 2013). Although the NHEJ of dysfunctional telomeres is abrogated in cells lacking 53BP1 or in cells expressing 53BP1^{28A} (Lottersberger et al., 2013), an allele harboring alanine substitutions at all 28 N-terminal ATM/ATR kinase phosphorylation targets sites, loss of RIF1 has considerably milder defect (Zimmermann et al., 2013). Moreover, although the generation of toxic radial chromosomes in BRCA1-deficient cells is prevented in 53BP1^{-/-} or in 53BP1^{28A} mutant cells (Bothmer et al., 2011; Bouwman et al., 2010; Bunting et al., 2012; Bunting et al., 2010), the loss of RIF1 only partially rescues HR in BRCA1-deficient cells (Escribano-Díaz et al., 2013; Feng et al., 2013; Zimmermann et al., 2013). This suggests that additional phosphorylation-dependent but RIF1-independent activities of 53BP1 might regulate the balance between HR and NHEJ.

PTIP is a ubiquitously expressed nuclear protein that associates constitutively with two of the known histone methyltransferases that catalyze trimethylation of histone H3 at lysine 4 (H3K4me3), MLL3, and MLL4 (Cho et al., 2007; Patel et al., 2007). In addition to its well-established role in transcription initiation, a separate pool of PTIP functions in an unknown capacity in the DDR (Gong et al., 2009). Indeed, PTIP has been implicated in both HR (Wang et al., 2010) and NHEJ (Callen et al., 2012). PTIP is recruited to DSBs by its tandem BRCT (BRCA1 carboxyl-terminal) domains (Manke et al., 2003; Yu et al., 2003), which associate with the serine 25 phosphorylation site within the N terminus of 53BP1 (Muñoz et al., 2007). In contrast to RIF1, PTIP recruitment to DSBs was reported to be 53BP1 and ATM independent (Gong et al., 2009; Jowsey et al., 2004; Muñoz et al., 2007). Thus, the mechanism by which PTIP is recruited to DSBs, its role in DSB repair, and the physiological significance of PTIP interaction with 53BP1 remain unclear. Here, we show that PTIP is required for 53BP1-mediated inhibition of HR in BRCA1-deficient cells but is dispensable for 53BP1-initiated DSB repair during productive CSR. Thus, RIF1 and PTIP separate 53BP1 functions in productive and pathologic DSB repair.

RESULTS

A Separation of Function Mutation in 53BP1

To determine whether 53BP1's activities in NHEJ and HR are distinct, we compared 53BP1^{8A}, which disrupts phosphorylation of the eight N-terminal ATM/ATR target sites (Figure 1A), to the 53BP1^{DB} allele, which is indistinguishable from WT 53BP1 in all functional aspects (Bothmer et al., 2011). To assay for CSR, BRCA1/53BP1-deficient B cells were transduced with wild-type and 53BP1 mutant proteins by retroviral infection after activation with lipopolysaccharide (LPS) and interleukin-4 (IL4). As expected, 53BP1^{DB} fully complemented the CSR

defects (Figure 1B) and produced high levels of genome instability in PARPi-treated BRCA1/53BP1-deficient cells (Figure 1C) (Bothmer et al., 2011). Surprisingly, despite rescuing CSR, the 53BP1^{8A} allele failed to promote genome instability in PARPi-treated BRCA1/53BP1-deficient cells above the levels observed in controls (Figure 1C). This effect was not due to differences in the expression levels of 53BP1 (Figure 1D) or in the recruitment of 53BP1 and RIF1 to DSBs (Figure 1E). Similar to B cells, BRCA1/53BP1-deficient MEFs complemented with 53BP1^{DB} were hypersensitive to PARPi, whereas 53BP1^{8A} transduced MEFs were not (Figure S1 available online). Thus, the mechanism by which 53BP1 promotes CSR and blocks HR in BRCA1-deficient cells is distinct. Moreover, the recruitment of RIF1 is insufficient to induce genome instability in PARPi-treated BRCA1-deficient cells.

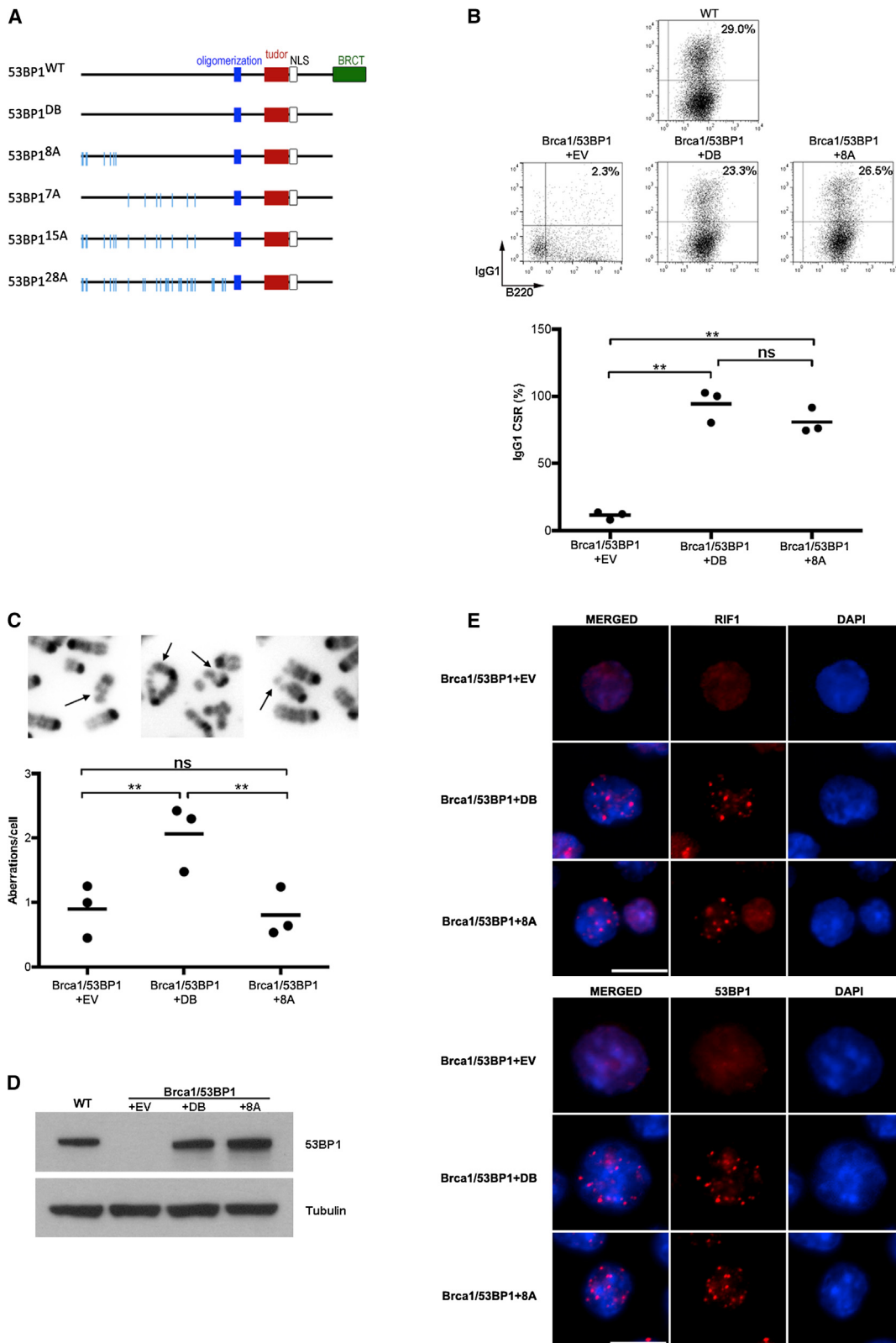
Role of PTIP in the DNA Damage Response

Upon DNA damage, PTIP binds to the serine 25 residue within the N terminus of 53BP1 (Muñoz et al., 2007), which is located within the eight N-terminal sites mutated in 53BP1^{8A}. Consistent with this, immunoprecipitation analysis revealed that PTIP association with 53BP1 after irradiation was abrogated in cells expressing S25A-harboring mutants 53BP1^{8A}, 53BP1^{15A}, or 53BP1^{28A} (Figures 2A and S2A). In contrast, the damage-induced 53BP1/PTIP interaction was maintained in the 53BP1^{7A} mutant, comprising alanine substitutions of 7 S/T/Q phosphorylation sites C terminus of those mutated in 53BP1^{8A} (Figures 1A and S2A).

To explore the function of PTIP in the DDR, we asked whether PTIP-deficient cells are sensitive to DNA damaging agents that are predominantly repaired by HR (Sonoda et al., 2006). WT and *PTIP*^{-/-} MEFs were exposed to either cisplatin, camptothecin, or PARPi, all of which sensitize HR-deficient cells (Bryant et al., 2005; Farmer et al., 2005). Each of these agents induced a similar level of chromosomal aberrations and reduction in cell survival in WT and *PTIP*^{-/-} MEFs (Figures 2B, 2C, and S2B). In contrast, *PTIP*^{-/-} MEFs were sensitive to irradiation (IR) (Figures 2B, 2C, and S2B) (Gong et al., 2009; Jowsey et al., 2004; Muñoz et al., 2007). Moreover, 53BP1^{8A} MEFs exhibited increased genome instability and reduced cell survival following IR (Figures S2C and S2D). To examine the recruitment of HR proteins to DSBs, we evaluated BRCA1, RAD51, and γ-H2AX foci formation after IR in WT and *PTIP*^{-/-} MEFs. All of these factors were normally recruited to DSBs in PTIP-deficient cells (Figure S2E). Moreover, 53BP1 also formed robust foci in the absence of PTIP (Figure S2E). Thus, *PTIP*^{-/-} MEFs are tolerant to agents that are highly toxic to HR-deficient cells and the recruitment of several factors implicated in DSB repair is intact in the absence of PTIP. Nevertheless, both *PTIP*^{-/-} and 53BP1^{8A} MEFs are sensitive to IR.

PTIP Is Dispensable for NHEJ during CSR but Is Required for NHEJ of Dysfunctional Telomeres

To explore the role of PTIP in NHEJ, we first assayed CSR. Deletion of PTIP in B cells leads to a defect in class switching to IgG3, IgG2b, and IgG1 (Daniel et al., 2010; Schwab et al., 2011). By recruiting an MLL-like methyltransferase complex to the switch regions of these isotypes, PTIP promotes histone modifications



(legend on next page)

and transcription initiation of IgG3/IgG2b/IgG1 germline switch regions, which are necessary for AID targeting (Daniel et al., 2010; Schwab et al., 2011). However, PTIP does not affect transcription at Igμ and Igε (Daniel et al., 2010), indicating that PTIP-associated methyltransferase complex promotes the accessibility of some but not all switch loci. To distinguish between PTIP's effects on transcription versus DSB repair, we compared CSR to IgG1 and IgE on day 5 after stimulation with αCD40+IL4 as described (Wesemann et al., 2011). As expected *PTIP*^{ff} *CD19*^{CRE} (*PTIP*^{-/-}) B cells displayed a defect in switching to IgG1 (Figures 3A and 3B), which is consistent with decreased *Igγ1* germline transcription (Daniel et al., 2010; Schwab et al., 2011). However, there was no defect in IgE germline transcription (Daniel et al., 2010) or IgE CSR in PTIP-deficient cells (Figures 3A and 3B). Indeed, IgE CSR was consistently higher in the absence of PTIP, likely because S_γ1 is no longer a target for AID. In contrast to *PTIP*^{-/-}, ablation of RIF1 in *Rif1*^{ff} *CD19*^{CRE} (*RIF1*^{-/-}) B cells impaired CSR to both IgG1 and IgE (Figures 3A and 3B). We conclude that loss of PTIP phenocopies the 53BP1^{8A} mutant allele in that neither has a significant impact on NHEJ during CSR.

An alternative end-joining pathway can catalyze substantial CSR end-joining to IgG1 and IgE even in the absence of classical NHEJ (Boboila et al., 2010). Loss of PTIP leads to IR sensitivity but tolerance to agents that are repaired by HR. We therefore speculated that PTIP might function in other reactions besides CSR that might rely on classical NHEJ, such as the fusion of dysfunctional telomeres. When the shelterin factor TRF2 is removed, deprotected telomeres trigger ATM-dependent phosphorylation of 53BP1, and the ends are processed by NHEJ to generate chromosome fusions (Celli et al., 2006; Rai et al., 2010; Zimmermann et al., 2013). Because ATM-dependent phosphorylation of 53BP1 is also required for interaction between 53BP1 and PTIP (Figures 2A and S2A) (Jowsey et al., 2004; Manke et al., 2003), we asked whether PTIP promotes NHEJ-mediated fusion of deprotected telomeres. To address this, we uncapped telomeres in SV40-immortalized WT and *PTIP*^{-/-} MEFs by removing TRF2 with short hairpin RNA against TRF2 (Rai et al., 2010). Upon TRF2 depletion we observed a similar level of phosphorylation of the ATM target KAP-1 in WT and *PTIP*^{-/-} MEFs, as measured by quantitative flow cytometry (Figure 4A). Consistent with this, there was an accumulation of cytologically discernable telomere-induced DNA damage foci (TIFs) containing γ-H2AX in WT and *PTIP*^{-/-} cells (Figure 4B). Despite a robust DNA damage response and activation of

ATM, the frequency of end-end chromosomal fusions was reduced by 2.8-fold in *PTIP*^{-/-} MEFs relative to WT (Figures 4C and 4D). Whereas 42% of WT cells bearing fusions had more than 30% of their chromosome ends fused, only 13% of PTIP KO cells had greater than 30% of their ends fused (Figure 4E). Thus, PTIP deficiency results in a reduction in the number of long-chain telomere fusions when telomeres are deprotected. We conclude that PTIP contributes to the NHEJ of dysfunctional telomeres.

PTIP Promotes Genome Instability in BRCA1-Deficient Cells

In contrast to 53BP1, loss of RIF1 only partially reverses the chromosomal aberrations and hypersensitivity produced by PARPi treatment of BRCA1-deficient cells (Escribano-Díaz et al., 2013; Zimmermann et al., 2013). To determine whether PTIP could overcome the HR defects in BRCA1-deficient cells, we crossed *PTIP*^{ff} and *BRCA1*^{f(Δ11)/f(Δ11)} mice with *CD19* CRE transgenic mice to simultaneously delete PTIP and exon 11 of BRCA1 in primary B lymphocytes. When unchallenged, *BRCA1*^{+/+} *PTIP*^{+/+} *CD19*^{CRE} (WT), *BRCA1*^{f(Δ11)/f(Δ11)} *CD19*^{CRE} (*BRCA1*^{-/-}), *PTIP*^{ff} *CD19*^{CRE} (*PTIP*^{-/-}), and *BRCA1*^{f(Δ11)/f(Δ11)} *PTIP*^{ff} *CD19*^{CRE} (*BRCA1*^{-/-} *PTIP*^{-/-}) doubly deficient B cells divided normally as determined by carboxyfluorescein succinimidyl ester (CFSE) dye dilution (Figure 5A) and cell-cycle distribution (Figure 5B). Treatment with PARPi did not impair the proliferation of WT or *PTIP*^{-/-} B cells (see also Figures 2B and 2C); however, *BRCA1*^{-/-} cells underwent fewer divisions over the course of 72 hr (Figure 5A). In contrast, loss of PTIP completely reversed the *BRCA1*^{-/-} growth defect (Figure 5A). Strikingly, although PARPi treatment generated chromatid breaks, chromosome breaks, and radial chromosomes in BRCA1-deficient cells (Bunting et al., 2010), *BRCA1*^{-/-} *PTIP*^{-/-} B cells were insensitive to PARPi (Figure 5C). Thus, ablation of PTIP phenocopies both the 53BP1^{8A} mutation (Figure 1C) and 53BP1 deficiency (Bouwman et al., 2010; Bunting et al., 2010; Cao et al., 2009) in that it promotes genome stability and survival in BRCA1 mutant cells.

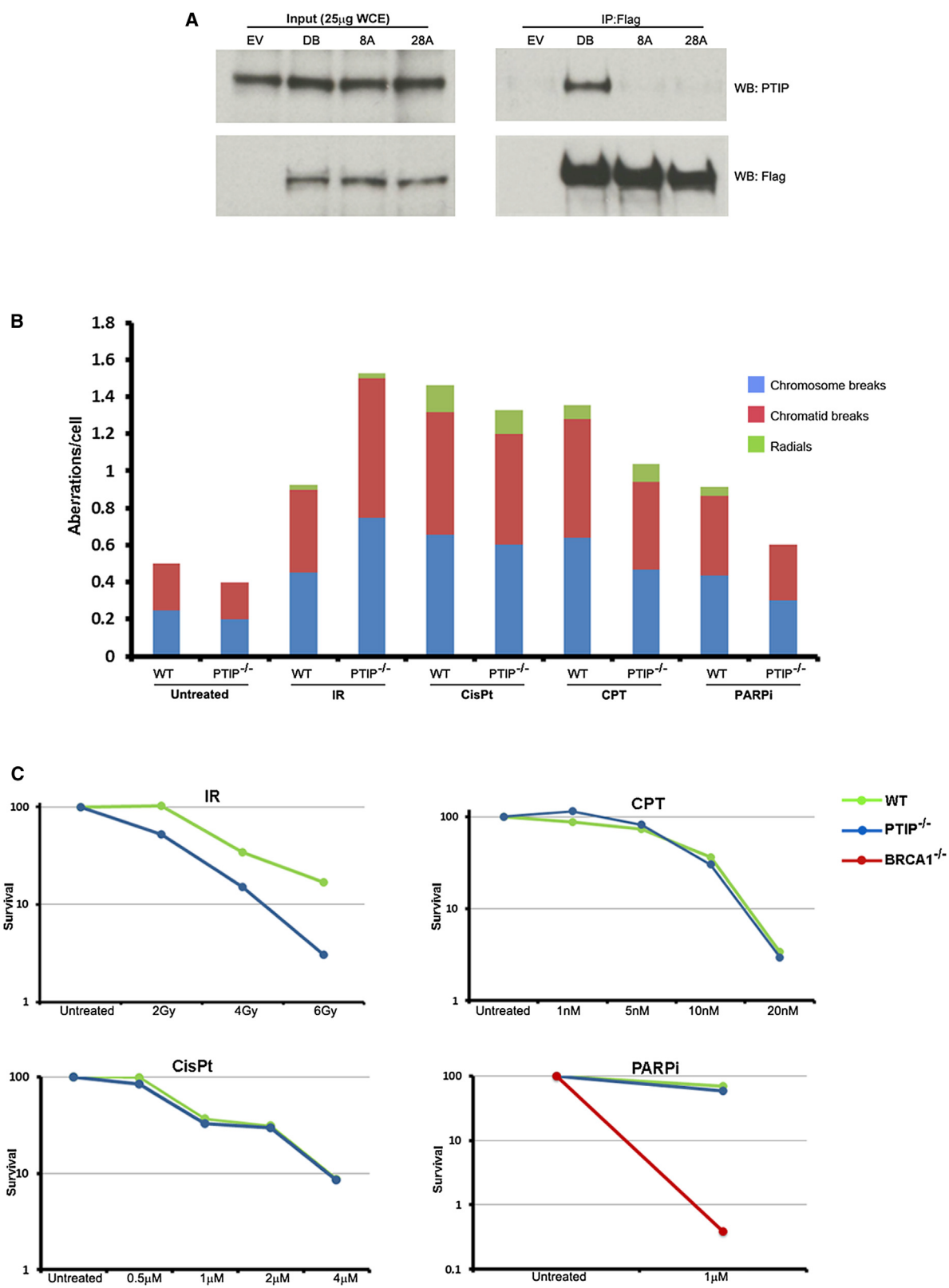
Loss of PTIP Increases HR in BRCA1 Mutant Cells by Promoting DSB Resection

BRCA1 and RAD51 function in a common HR pathway that promotes RAD51-mediated DNA strand exchange (Bhattacharya et al., 2000; Moynahan et al., 1999; Scully et al., 1997). Loss of 53BP1 rescues RAD51 foci formation and HR in

Figure 1. Characterization of a Separation of Function Mutant 53BP1

- (A) Diagram of the 53BP1 retroviral constructs used. Hash marks indicate location of substituted S/TQ sites.
- (B) Top: Representative flow cytometry plots measuring CSR after stimulation of WT and *BRCA1*^{-/-} *53BP1*^{-/-} B cells infected with retroviruses expressing 53BP1^{DB} (amino acids 1–1710), the N-terminal mutant 53BP1^{8A} or empty vector (EV). Numbers represent the percentages of IgG1 switched cells. B220 is a B cell marker. Bottom: Dot plot indicating IgG1 CSR as a percentage of WT value in the same experiment. Three independent experiments are shown. **p < 0.001 (two-tailed unpaired t test); *BRCA1*/53BP1+DB versus *BRCA1*/53BP1+8A, p > 0.1, which is not significant (ns).
- (C) *BRCA1*^{-/-} *53BP1*^{-/-} B cells were reconstituted with empty vector, 53BP1^{DB} and 53BP1^{8A} retroviruses and treated with PARPi. The arrows indicate representative images of aberrant chromosomes. Dot plot indicates the total aberrations per cell in three independent experiments. At least 50 metaphases were analyzed for each genotype in each experiment. **p < 0.01 (two-tailed unpaired t test); ns: not significant.
- (D) Western blot analysis of 53BP1 expression in WT B cells and *BRCA1*^{-/-} *53BP1*^{-/-} B cells stimulated and infected with empty vector, 53BP1^{DB}, or 53BP1^{8A}.
- (E) *BRCA1*^{-/-} *53BP1*^{-/-} B cells infected with EV, 53BP1^{DB} or 53BP1^{8A} retroviruses were assayed for IRIF (10 Gy, 2 hr recovery) for RIF1 (red, top), and 53BP1 (red, bottom). Cells were counterstained with DAPI (blue). Scale bar, 10 μm.

See also Figure S1.



(legend on next page)

BRCA1-deficient cells (Bouwman et al., 2010; Bunting et al., 2010). To explore whether PTIP deficiency also promotes HR in BRCA1-deficient cells, we irradiated WT, *BRCA1*^{-/-}, *PTIP*^{-/-}, and *BRCA1*^{-/-}*PTIP*^{-/-} B cells and measured the frequency of immunofluorescent RAD51 foci. All mutant cells proliferated similarly to WT over the course of 3 days (Figure 5A), and as expected, RAD51 foci were reduced in IR-treated *BRCA1*^{-/-} cells (Figure 5D). However, in *PTIP*^{-/-} cells, the frequency of RAD51 foci was greater than WT, and RAD51 foci were normalized to WT levels in *BRCA1*^{-/-}*PTIP*^{-/-} B cells (Figure 5D). These results suggest that loss of PTIP reverses the HR defect in BRCA1-deficient cells, thereby explaining the insensitivity of *BRCA1*^{-/-}*PTIP*^{-/-} B cells to PARPi.

Loss of PTIP might promote RAD51 foci formation by allowing increased resection of DSBs; this is similar to what happens with the loss of 53BP1 (Bunting et al., 2010; Difilippantonio et al., 2008). Because 5'→3' DSB end resection produces RPA-coated single-strand DNA, we monitored RPA foci formation by high content microscopy. Irradiated *PTIP*^{-/-} cells exhibited a significant increase in the mean number of RPA foci per cell relative to WT (Figure 5E); moreover, the fraction of *PTIP*^{-/-} cells that had more than 15 RPA foci following IR was approximately 2-fold greater than WT (Figure 5E). Thus, PTIP limits the amount of chromatin bound RPA at IR-induced DSBs.

PTIP Recruitment to DSBs Promotes Radial Chromosomes in BRCA1-Deficient Cells

PTIP is a subunit of the MLL3/4 methyltransferase complex and promotes histone H3 lysine 4 trimethylation and transcription initiation at specific promoters, such as the Sy3/Sy1 switch regions of the *Igh* locus (Daniel et al., 2010) (Figure S3A). To determine whether transcription of DDR genes is altered by PTIP ablation, we profiled the transcriptome of WT and *PTIP*^{-/-} B cells. Overall, there were 471 RefSeq annotated genes that were deregulated by more than 5-fold in *PTIP*^{-/-} versus WT (Figure S3B). However, HR and NHEJ DNA damage response genes were not among deregulated pathways (Figures S3B and S3C). This suggests that the functions of PTIP in suppressing HR might be unrelated to its role in transcriptional regulation.

To determine whether PTIP recruitment to DSBs is essential for its effects on HR, we made use of a point mutation in the BRCT domain 3 (W663R) of PTIP that selectively blocks its interaction with 53BP1 (Gong et al., 2009; Munoz et al., 2007) and is unable to form foci (Figure S4A) (Daniel et al., 2010) but retains PTIP association with the MLL3/4 complex, which is

dependent on BRCT (domains 5 and 6) (Patel et al., 2007). *BRCA1*^{-/-}*PTIP*^{-/-} B cells were infected with PTIP^{WT} and PTIP^{W663R} encoding retroviruses, treated with PARPi, and monitored for chromosomal damage (Figures 5F and S4B). Whereas PTIP^{WT} expression in *BRCA1*^{-/-}*PTIP*^{-/-} cells led to an increase in the number of chromosomal radials relative to uninfected cells, *BRCA1*^{-/-}*PTIP*^{-/-} cells transduced with PTIP^{W663R} remained insensitive (Figures 5F and S4B). Thus, PTIP recruitment to DSBs is necessary to block HR in BRCA1-deficient cells.

Recruitment of PTIP to DSBs Is Dependent on the Eight Most N-Terminal S/TQ Phosphorylation Sites of 53BP1

To explore the mechanism of PTIP recruitment to DSBs, we expressed FLAG-tagged PTIP in WT, 53BP1^{-/-}, and ATM^{-/-} MEFs and irradiated them with 10 Gy (Figure 6A). Although PTIP ionizing-irradiation-induced foci (IRIF) were detectable in nearly all WT cells, PTIP IRIF formation was impaired in the absence of 53BP1 or ATM (Figure 6A). Measurements of colocalization coefficients of γ-H2AX (a marker of the DNA breaks) with PTIP in irradiated WT, 53BP1^{-/-}, and ATM^{-/-} MEFs revealed that 80% of γ-H2AX foci in WT cells contained PTIP, whereas less than 15% and 10% of γ-H2AX foci in the 53BP1^{-/-} and ATM^{-/-} cells, respectively, contained PTIP. Consistent with these findings, PTIP IRIF was highly sensitive to pharmacological inhibition of ATM (ATMi), less sensitive to ATRi treatment, and insensitive to DNA-PK. (Figure S5). These findings contrast with previous reports suggesting that PTIP, 53BP1, and ATM are independently recruited to DSBs (Gong et al., 2009; Jowsey et al., 2004; Munoz et al., 2007). Because available PTIP antibodies are unable to detect endogenous PTIP foci, we used laser microirradiation to generate DSBs in WT, 53BP1^{-/-}, and ATM^{-/-} MEFs. In WT cells, PTIP was recruited to laser scissors-induced DSBs, which colocalized with γ-H2AX (Figure 6B). Consistent with our analysis of IRIF, PTIP recruitment to DNA damage sites was 53BP1 and ATM dependent (Figure 6B). Moreover, PTIP failed to be recruited to DSBs in 53BP1^{-/-} MEFs reconstituted with a mutant protein lacking all 28 N-terminal S/TQ phosphorylation sites of 53BP1, 53BP1^{28A} (Figure 6B). We conclude that ATM-dependent phosphorylation of 53BP1 is necessary for PTIP recruitment to DSBs.

Given that RIF1 is also recruited to DSBs in a 53BP1- and ATM-dependent manner (Chapman et al., 2013; Di Virgilio et al., 2013; Escribano-Díaz et al., 2013; Feng et al., 2013; Silverman et al., 2004; Zimmermann et al., 2013), we next monitored the codependency of PTIP and RIF1 for localization to DNA damage foci (Figure 6C). We found that 82% of PTIP IRIF colocalized

Figure 2. Response of PTIP to Different DNA Damaging Agents

(A) 53BP1^{-/-} B cells were reconstituted with empty vector, 53BP1^{DB}, 53BP1^{28A}, or 53BP1^{28A} retroviruses that were FLAG-tagged. Cells were irradiated (10 Gy, 45 min recovery) and immunoprecipitation was performed with anti-FLAG antibodies. Western blot analysis of PTIP and FLAG are shown for input (left) and immunoprecipitated protein (right).

(B) Isogenic immortalized WT and *PTIP*^{-/-} MEFs were either untreated or treated with irradiation (IR, 2 Gy), cisplatin (CisPt, 0.5 μM), camptothecin (CPT, 10 nM) or PARP inhibitor (PARPi, 1 μM) and chromosomal aberrations (chromatid breaks, chromosome breaks, and radials) were quantified in at least 50 metaphase spreads for each genotype and each treatment. Data from an independent experiment is shown in Figure S2B.

(C) WT (green lines) and *PTIP*^{-/-} (blue line) MEFs were treated with different doses of the above drugs, and colony formation was quantified relative to colonies formed in untreated cells from the same genotype. An experiment performed in parallel demonstrated that 1 μM PARPi treatment is toxic for BRCA1 mutant MEFs (red line).

See also Figure S2.

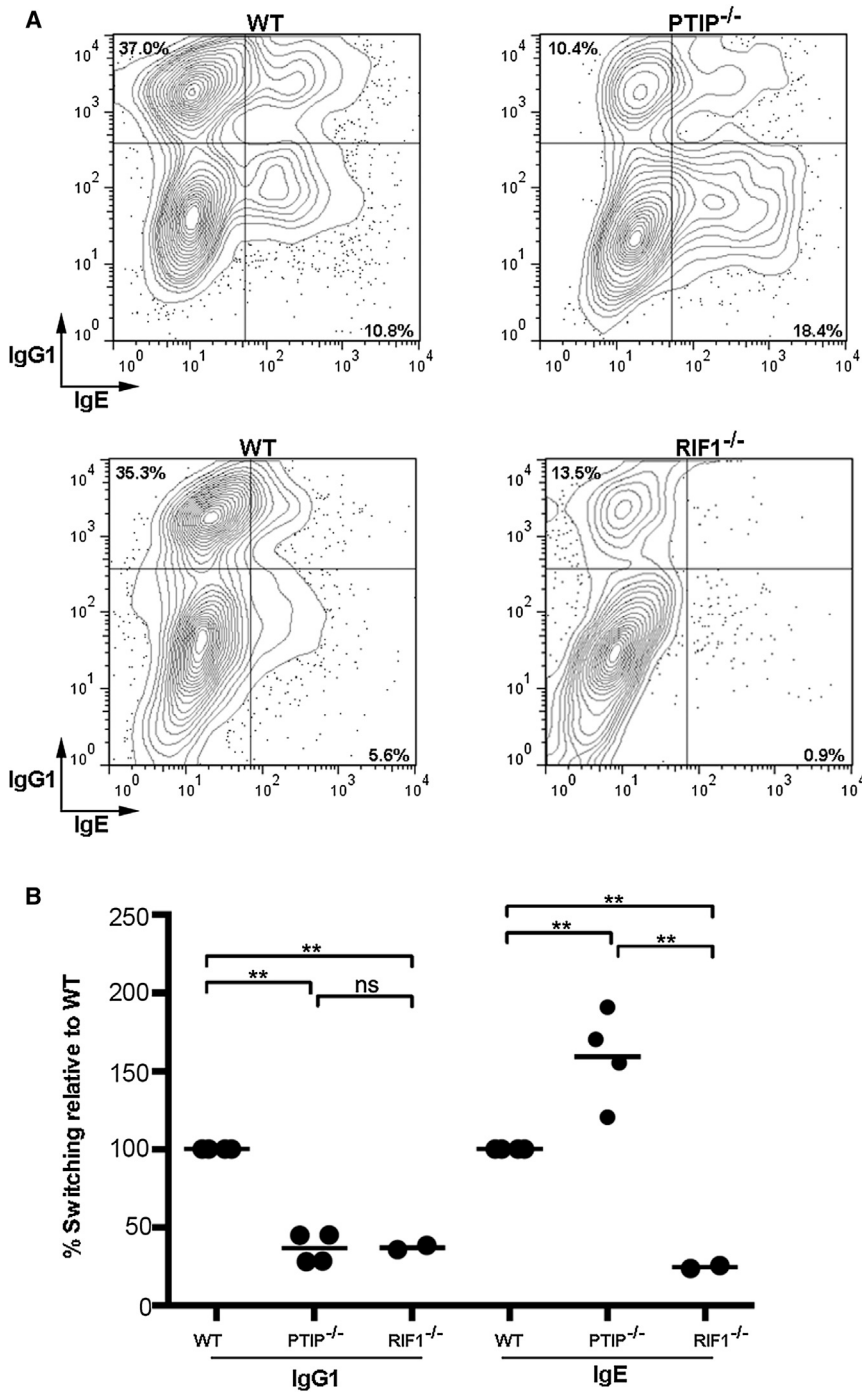


Figure 3. PTIP Is Dispensable for CSR to IgE
PTIP^{fl/fl}CD19^{CRE} (*PTIP^{-/-}*), (*Rif1^{fl/fl}CD19^{CRE}*) *RIF1^{-/-}* and littermate WT B cells were stimulated with α CD40 plus IL-4 and analyzed for IgG1 and IgE CSR on day 5.

(A) Representative flow cytometry plots. The percentages of IgG1 switched cells (upper-left quadrant) and IgE switched cells (lower-right quadrant) is indicated.

(B) Dot plot indicates IgG1 and IgE CSR in *PTIP^{-/-}* and *RIF1^{-/-}* as a percentage of the WT value in the same experiment. ** $p < 0.01$ (two-tailed unpaired t test); ns: not significant.

S2A). Whereas expression of 53BP1^{DB} in 53BP1^{-/-} MEFs reconstituted PTIP IRIF (Figures 7A and S6A), PTIP recruitment to DSBs was abrogated in 53BP1^{8A} MEFs (Figures 7A and S6A). By contrast, RIF1 recruitment was independent of these eight most N terminus phosphorylation sites on 53BP1, partially dependent on the seven S/TQ phosphorylation sites C terminus to 53BP1^{8A}, and abrogated in 53BP1^{15A} mutant cells that lack all 8S/TQ and 7S/TQ phosphorylation sites (Figures 7A–7C and S6B). Thus, PTIP and RIF1 exhibit distinct phosphorylation-dependent interactions with 53BP1 that guide them to DSBs. The association of PTIP with the 8S/TQ sites on 53BP1 upon DNA damage (Figures 2A, 7, and S6A) likely explains why loss of PTIP phenocopies 53BP1^{8A} with respect to CSR, irradiation sensitivity, and reversal of genome instability in BRCA1-deficient cells.

DISCUSSION

Regulation of DSB Repair Choice

53BP1 and BRCA1 play a critical role in channeling DSBs into either NHEJ or HR. 53BP1 promotes NHEJ in G1 by tethering DSBs together and by protecting these ends from exonuclease processing (Bothmer et al., 2010; Difilippantonio et al., 2008). In S phase, the inhibitory effect of 53BP1 on resection is antagonized by BRCA1 (Bouwman et al., 2010; Bunting et al., 2010). Loss of BRCA1 results

in a shift toward a mutagenic NHEJ pathway that results in chromosomal abnormalities, tumorigenesis, and embryonic lethality, but all of these phenotypes are relieved by 53BP1 deletion (Bouwman et al., 2010; Bunting et al., 2010; Cao et al., 2009). In contrast, loss of classical NHEJ proteins (e.g., Ku, Ligase IV, DNA-PKcs) does not overcome the HR defects associated with BRCA1 deficiency (Bunting et al., 2012; Bunting et al., 2010), perhaps because these factors play a more limited role

with RIF1 foci and 78% of RIF1 colocalized with PTIP foci (Figure 6C, $n > 800$ foci). However, RIF1 was recruited to DNA damage sites in *PTIP^{-/-}* MEFs (Figure 6D) and vice versa (Figure 6E). Thus, RIF1 and PTIP are independently recruited to IRIF in a phospho-53BP1-dependent manner.

To further define the residues required for recruitment to phospho-53BP1, we examined PTIP and RIF1 recruitment in 53BP1^{DB}, 53BP1^{8A}, and 53BP1^{7A} mutant MEFs (Figures 2A and

in repressing 5'-3' resection (Bunting et al., 2012; Sfeir and de Lange, 2012). Despite the striking rescue of BRCA1 deficiency, disrupting 53BP1 does not reverse the DNA repair defects associated with downstream mediators of the HR reaction (e.g., XRCC2, BRCA2, or PALB2) (Bouwman et al., 2010; Bowman-Colin et al., 2013; Bunting et al., 2010). Thus, 53BP1 and BRCA1 oppose each other during critical initial stages of DSB repair before commitment to repair the ends by NHEJ or HR.

Mechanism of PTIP and RIF1 Association with 53BP1

The molecular events that are required for 53BP1 to promote the ligation of DNA ends during CSR and the aberrant chromosomal rearrangements in BRCA1 mutant cells were previously thought to be identical. Surprisingly our data suggest that the pro-NHEJ and anti-HR functions of 53BP1 are in fact distinct and separable activities that nevertheless require 53BP1 phosphorylation. These complementary aspects of 53BP1's activities are mediated by the independent recruitment of RIF1 and PTIP, respectively, to phosphorylated 53BP1.

PTIP contains BRCT domains that interact directly with phosphorylated 53BP1 (Manke et al., 2003; Munoz et al., 2007). In contrast, RIF1 does not contain a known phosphorecognition motif, and it remains unclear how ATM-dependent phosphorylation facilitates RIF1 association with 53BP1. RIF1 may associate with 53BP1 directly or through interactions with effector molecules that contain BRCT phosphobinding modules (Figure 7D). Based on the observation that there is no detectable defect in RIF1 foci in 53BP1^{8A} cells (Figures 7A and S6B), we suspected that a major RIF1-interaction motif would reside C terminus of the 8S/TQ PTIP interaction sites. Consistent with this, the 53BP1^{7A} C-terminal mutant exhibits a reduction in RIF1 IRIF (Figures 7A–7C) and CSR (Bothmer et al., 2011). RIF1 IRIF and CSR are further reduced in 53BP1^{15A} mutant cells that lack 8S/TQ and 7S/TQ sites (Figures 7A and 7B) (Bothmer et al., 2011), suggesting that both regions contribute to RIF1 interactions with 53BP1 (Figure 7D). If so, we would predict some degree of competition between PTIP and RIF1 binding to 53BP1. Consistent with this, we have found an increased association between PTIP and 53BP1 in response to DNA damage in RIF1-deficient cells (Figure S6C). Thus, distinct from PTIP, RIF1 association with 53BP1 occurs via multidomain interactions (Figure 7D).

Role of PTIP and RIF1 in DSB Resection

Deletion of either PTIP or RIF1 leads to increased resection (Figure 5E) (Chapman et al., 2013; Di Virgilio et al., 2013; Escribano-Díaz et al., 2013; Feng et al., 2013; Zimmermann et al., 2013). However, whereas PTIP ablation rescues HR in BRCA1-deficient cells and is largely dispensable for NHEJ during CSR, RIF1 is essential for CSR and only partially contributes to the HR defects in BRCA1-deficient cells (Di Virgilio et al., 2013; Escribano-Díaz et al., 2013; Feng et al., 2013; Zimmermann et al., 2013). How can these observations be reconciled? One possibility is that distinct S/TQ kinase target sites in 53BP1 are phosphorylated during CSR in G1 and during replication fork collapse in S, resulting in independent recruitment of the two factors to DNA ends in distinct phases of the cell cycle. Consistent with this idea, it was reported that the localization of RIF1 to DSBs is mainly restricted

to G1 and is suppressed by BRCA1 in S/G2 (Chapman et al., 2013; Escribano-Díaz et al., 2013; Feng et al., 2013). However, our finding that PTIP and RIF1 colocalize in the majority of irradiated cells and that both proteins form IRIF during G1 and S/G2 (Figure S7) indicates that PTIP and RIF1 are not recruited to DSBs in distinct cell-cycle phases.

Another possibility is that PTIP and RIF1 sites on 53BP1 are equally phosphorylated during the cell cycle but that these proteins might make the DSB-proximal chromatin refractory to a distinct set of nucleases. For example, initial DNA end resection is mediated by MRE11/RAD50/NBS1 and CTIP, whereas DNA2, EXO1, and BLM carry out more extensive resection (Symington and Gautier, 2011), and RIF1 appears to be involved in protection against initial but not sustained resection (Feng et al., 2013). In this model, the level of resection supported by loss of RIF1 would be insufficient for complete rescue of HR in *BRCA1*-deficient cells, which might require more extensive 3' single-strand tails. In contrast, ablation of PTIP supports the sustained resection required for the rescue of HR in *BRCA1*-deficient cells. Thus, RIF1 and PTIP may block different steps in resection or distinct nucleases that mediate HR.

Role of PTIP and RIF1 in Telomeric End-Joining

Depending on the nature of the break, RIF1 and PTIP might cooperate to promote NHEJ. For example, PTIP and RIF1 deficiency both result in IR sensitivity (Figures 2B and 2C) (Feng et al., 2013), and defective NHEJ of dysfunctional telomeres (Figure 4) (Chapman et al., 2013; Zimmermann et al., 2013). It has been demonstrated that 53BP1 has RIF1-independent roles in promoting telomeric end-joining, evidenced by the considerably higher frequency of telomeric fusions in *RIF1*^{-/-}*TRF2*^{-/-} versus *53BP1*^{-/-}*TRF2*^{-/-} or *53BP1*^{28A}*TRF2*^{-/-} MEFs (Lottersberger et al., 2013; Zimmermann et al., 2013). This RIF1-independent but phospho-53BP1-dependent function at telomeres has been linked to the induction of chromosome mobility (Zimmermann et al., 2013), which increases the probability that DNA ends fuse. Because PTIP binds to DSBs in a 53BP1-dependent but RIF1-independent manner, it is possible that this 53BP1-dependent/RIF1-independent increase in telomere mobility is mediated by PTIP.

Implications for Cancer Therapy

The identification of separation of function mutations that selectively disrupt antirecombination functions of 53BP1 during replication fork collapse and CSR may open up new therapeutic opportunities. Breast cancers arising in *BRCA1* mutation carriers frequently show low levels of 53BP1 expression (Bouwman et al., 2010), which might result in resistance to PARPi therapy, a promising strategy for treating HR-deficient tumors (Bryant et al., 2005; Farmer et al., 2005). Consistent with this, 53BP1 was lost in a fraction of *BRCA1*-deficient mouse mammary tumors that acquired PARPi resistance *in vivo* (Jaspers et al., 2013). Interestingly, a fraction of PARPi-resistant tumors restored HR yet did not lose 53BP1. We speculate that PTIP mutation might emerge as a novel causal factor in PARPi resistance of *BRCA1*-deficient mammary tumors that restore HR. With respect to intervention, our study also suggests that it might be possible to increase HR in *BRCA1* heterozygous carriers

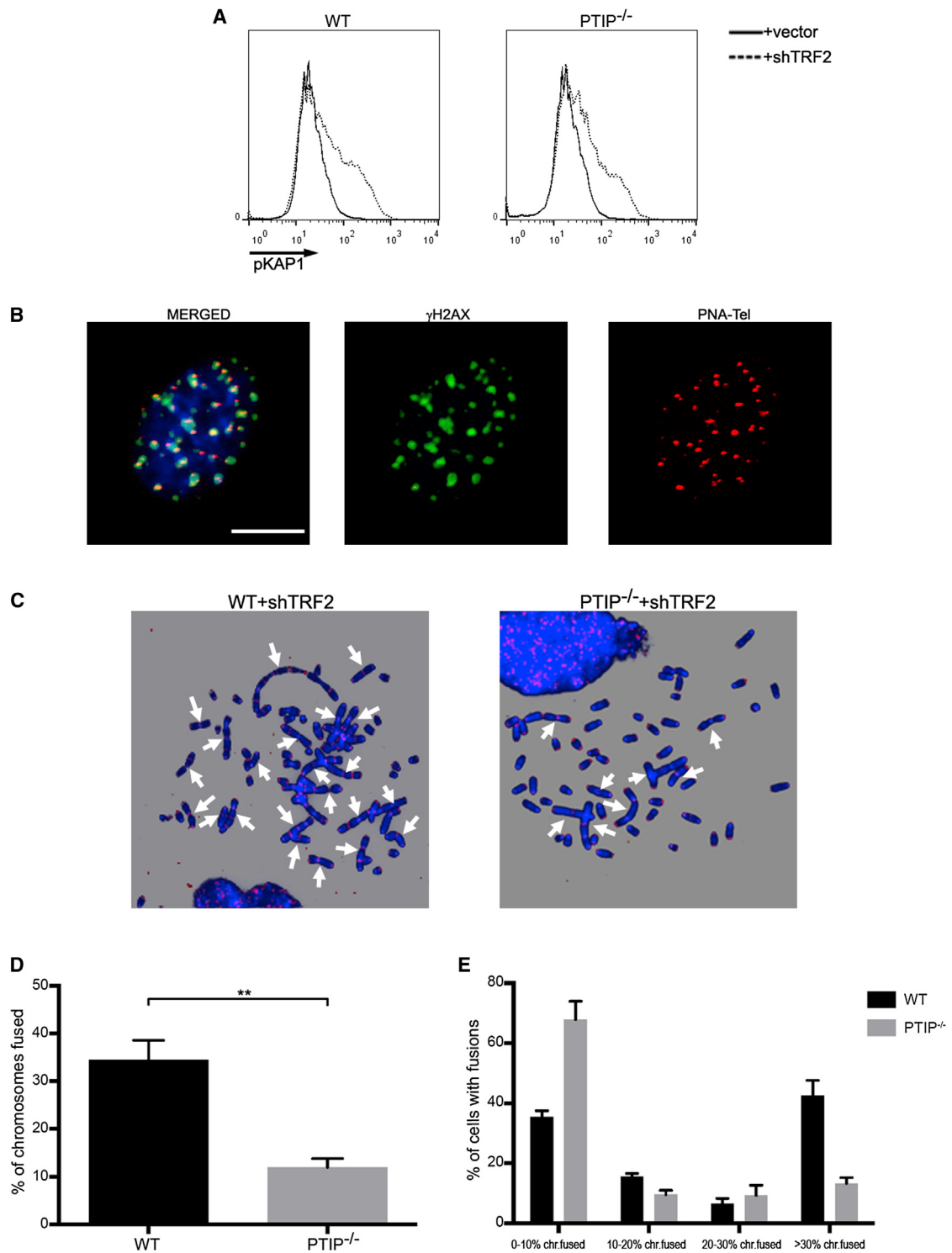


Figure 4. PTIP Is Required for NHEJ of Dysfunctional Telomeres

(A) WT and *PTIP*^{-/-} MEFs were infected with a retrovirus expressing either an empty vector or shRNA against TRF2 (shTRF2), and phosphorylated KAP1 (pKAP1) levels were measured by flow cytometry.

(B) γ -H2AX (green) in telomere-dysfunction-induced foci (TIF) generated in shTRF2-infected WT cells. PNA probe is shown in red, and images are merged on top of DAPI (blue). Scale bar, 10 μ m.

(C) Representative images of a metaphase spread from WT and *PTIP*^{-/-} MEFs infected with shTRF2. Telomere fusions are visualized by a telomeric PNA probe (red) and DAPI (blue). Arrows point to representative telomeric fusions.

(legend continued on next page)

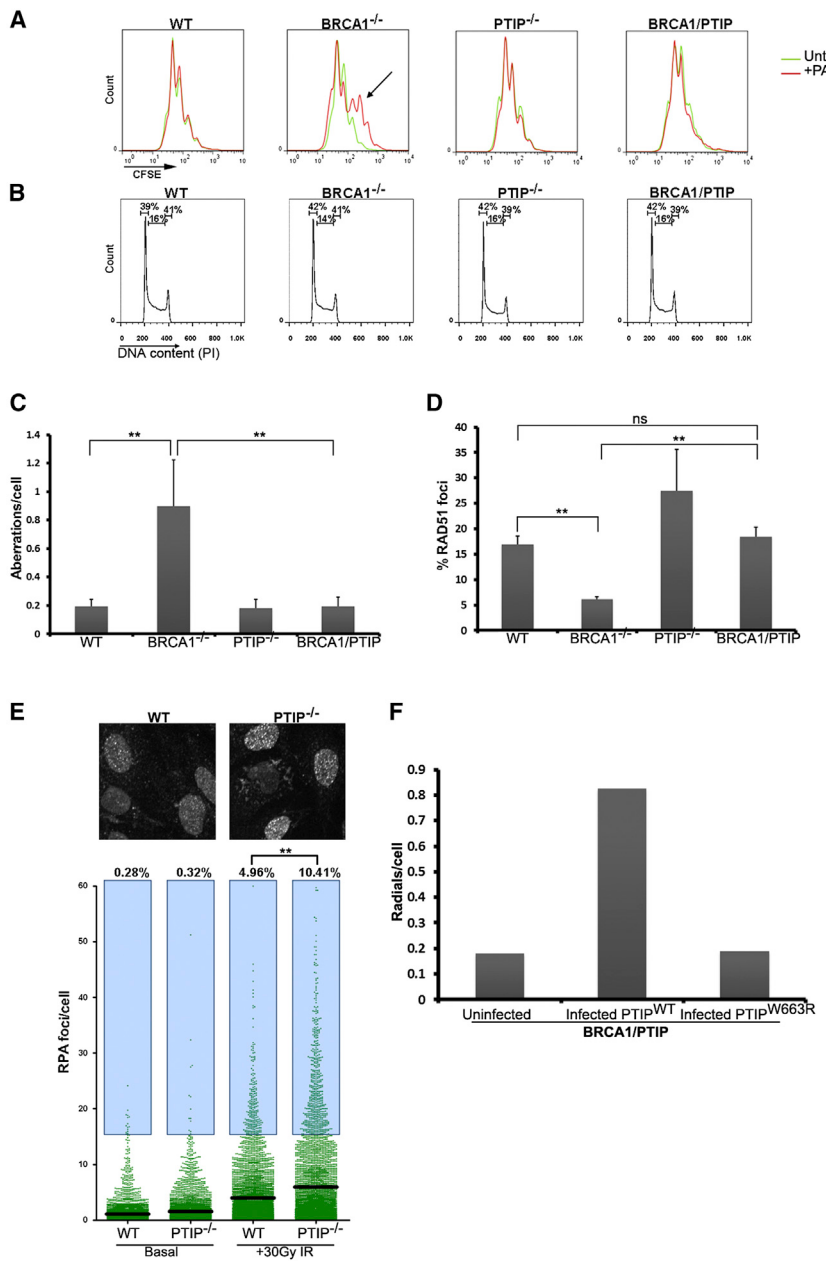


Figure 5. Ablation of PTIP Rescues Homologous Recombination in *BRCA1*-Deficient Cells

(A) WT, *BRCA1*^{-/-}, *PTIP*^{-/-}, and *BRCA1*^{-/-}/*PTIP*^{-/-} B cells were pulsed with CFSE and stimulated with (red) or without (green) PARPi. CFSE signal diminishes with increasing division. *BRCA1*^{-/-} cells are sensitive to PARPi (arrow indicates sluggish cells) but loss of PTIP in *BRCA1*-deficient cells rescues the proliferation defect.

(B) WT, *BRCA1*^{-/-}, *PTIP*^{-/-}, and *BRCA1*^{-/-}/*PTIP*^{-/-} B cells were stimulated with LPS+IL4 and cell-cycle distribution was monitored by propidium iodide (PI) staining. Percentage of cells in G1, S, and G2/M is indicated.

(C) Analysis of genomic instability (radial chromosomes, chromatid breaks, and chromosome breaks) in metaphases from B cells treated with 1 μ M PARPi. At least 50 metaphases were analyzed for each genotype.

(D) B cells were stimulated for 2 days, irradiated with 10 Gy, and the percentage of cells with immunofluorescent RAD51 foci were quantified (at least 400 cells counted for each genotype).

Data in (B) and (C) represent mean of three experiments \pm standard deviations. ** $p < 0.05$ (two-tailed unpaired t test), ns, not significant.

(E) High-throughput microscopy quantification of RPA foci per cell in WT and *PTIP*^{-/-} MEFs that were either untreated or treated with 30 Gy IR. Top: representative image of chromatin bound RPA in irradiated WT and *PTIP*^{-/-} cells. Bottom: quantitation of RPA foci. Bar indicates the mean number of RPA foci per cell, and the blue box designates cells with more than 15 foci, whose percentage is indicated above each box. ** $p < 0.001$.

(F) *BRCA1*^{-/-}/*PTIP*^{-/-} B cells were reconstituted with *PTIP*^{WT} or *PTIP*^{W663R} retroviruses (expressing a GFP marker driven by an internal ribosome entry site) and treated with PARPi. Cells were sorted (GFP^{positive} = infected and GFP^{negative} = uninfected) and metaphases were analyzed for radial chromosomes ($n = 50$ metaphases analyzed in each case).

See also Figures S3 and S4.

without compromising B cell immunoglobulin class switching by inhibiting the recruitment of PTIP to DSBs.

EXPERIMENTAL PROCEDURES

Mice, MEFs, B Cell Culture, and Infections

53BP1^{-/-} (Ward et al., 2004), *BRCA1*^{f(f11)/f(f11)} (NCI mouse repository), *RIF1*^{ff} (Buonomo et al., 2009; Di Virgilio et al., 2013), and *PTIP*^{ff} (Daniel et al., 2010)

mice have been described. Resting splenic B cells were isolated from 8- to 12-week-old WT or mutant spleen with anti-CD43 microbeads (anti-Ly48; Miltenyi Biotech) and were cultured with LPS (25 μ g/ml; Sigma) and IL-4 (5 ng/ml; Sigma) or α CD40 (1 μ g/ml; eBiosciences) and IL4 as described (Barlow et al., 2013; Wesemann et al., 2011). WT, 53BP1^{-/-}, and ATM^{-/-} MEFs were immortalized by SV40. SV40T immortalized *PTIP*^{ff} (Cho et al., 2009) and *RIF1*^{ff} MEFs were infected with CRE viruses to delete PTIP and RIF1, respectively. PMX-PIE-based retroviruses encoding 53BP1^{DB} and 53BP1^{8A} were previously described (Bothmer et al., 2011). Coding sequences

(D) Quantitation of telomeric fusion frequencies. At least 1,800 chromosomes from each genotype were analyzed. Mean value derived from three independent experiments. ** $p < 0.01$ (two-tailed unpaired t test). Error bars represent SEM.

(E) Distribution of telomeric fusions per metaphase in WT and *PTIP*^{-/-} MEFs. At least 30 cells were examined in each of three independent experiments. $p(\chi^2) < 1 \times 10^{-5}$. Error bars represent SEM.

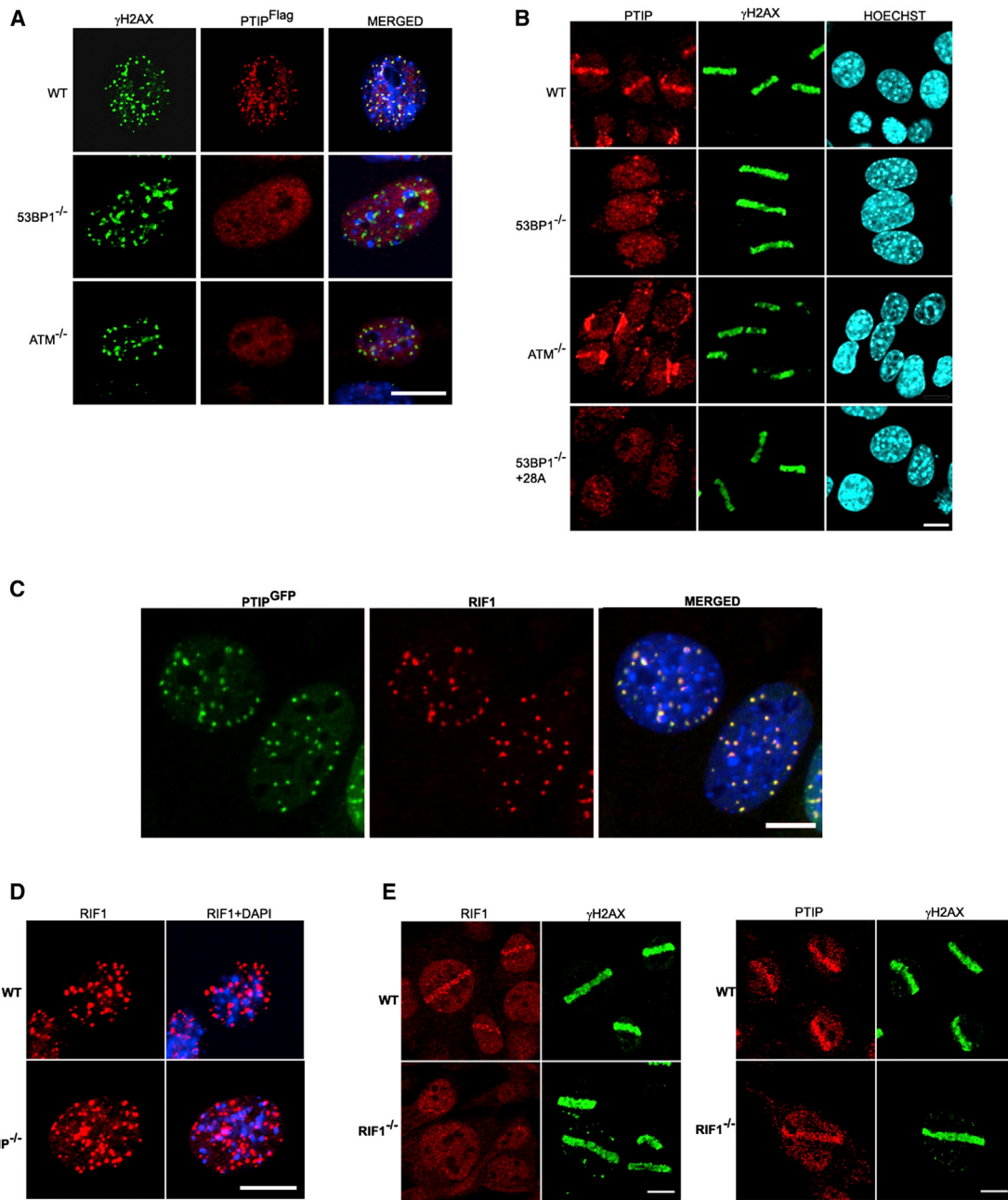


Figure 6. Recruitment of PTIP to DSBs Is ATM and Phospho-53BP1-Dependent but RIF1-Independent

(A) WT, $53BP1^{-/-}$, and $ATM^{-/-}$ MEFs were infected with a FLAG-tagged WT PTIP retrovirus. Cells were irradiated with 10 Gy, and FLAG (red) IRIF together with γ -H2AX (green) were assessed 4 hr post-IR. DAPI is indicated in blue.

(B) WT, $53BP1^{-/-}$, $ATM^{-/-}$, and $53BP1^{-/-} + 28A$ MEFs reconstituted with $53BP1^{28A}$ were treated with Hoechst 33342 and then irradiated with a 364 nm laser line. Cells were allowed to recover for 15 min before processing for immunofluorescence analysis of PTIP and γ -H2AX. Hoechst counterstain is indicated in blue.

(C) Cells expressing GFP-PTIP were irradiated with 10 Gy, and PTIP^{GFP} (green) and RIF1 (red) IRIF were assessed 4 hr later. A representative image is shown; 82% of PTIP IRIF colocalized with RIF1 foci and 78% of RIF1 colocalized with PTIP foci ($n \geq 800$ foci examined; cells had on average 28 foci).

(D) RIF1 IRIF (red) in irradiated WT and $PTIP^{-/-}$ MEFs.

(E) RIF1 (red) and PTIP (red) recruitment to laser scissors damage in WT and $RIF1^{-/-}$ MEFs. Damaged cells are indicated by γ -H2AX tracks (green). Scale bars, 10 μ m.

See also Figure S5.

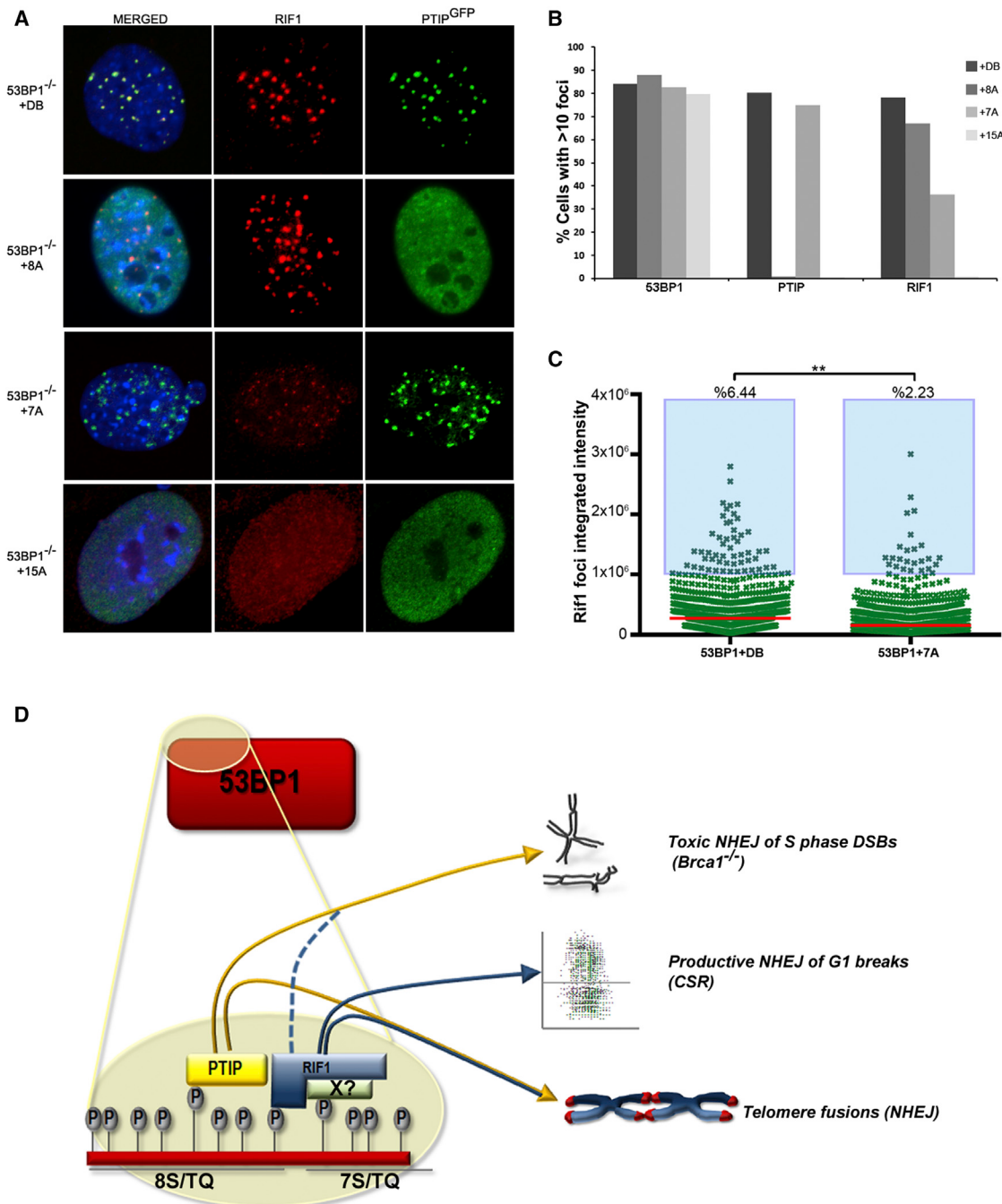


Figure 7. PTIP and RIF1 Association with DSBs Is Dependent on Distinct Phosphorylation Sites on 53BP1

(A) $53BP1^{-/-}$ MEFs (reconstituted with $53BP1^{DB}$, $53BP1^{8A}$, $53BP1^{7A}$, or $53BP1^{15A}$) were costained with RIF1 (red) and PTIP (green).

(B) Quantitation of percent $53BP1^{DB}$, $53BP1^{8A}$, $53BP1^{7A}$, or $53BP1^{15A}$ cells with greater than ten $53BP1$, PTIP, or RIF1 foci. At least 100 cells were analyzed for each genotype.

(C) Integrated intensity of individual RIF1 foci in $53BP1^{-/-}$ MEFs reconstituted with DB or 7A. Average RIF1 foci intensity (red line) is 1.6-fold greater in DB versus 7A (** $p < 0.001$, one-tailed unpaired t test), and a greater percentage of very intense foci (z score > 3) are generated in $53BP1^{DB}$ compared to $53BP1^{7A}$ (blue box).

(D) Model for regulation of $53BP1$ pro-NHEJ and anti-HR activities by distinct phosphointeractions with RIF1 and PTIP, respectively. PTIP binds to the 8S/TQ sites. RIF1 recruitment is largely dependent on C-terminal 7S/TQ sites, but RIF1 may also be stabilized by interactions with 8S/TQ. An unknown factor (X) may bind directly to phosphorylated $53BP1$ and mediate RIF1 recruitment, whereas PTIP interaction with $53BP1$ is direct (Muñoz et al., 2007).

See also Figures S6 and S7.

for mouse PTIP^{WT}/PTIP^{W663R} and PTIP-GFP were cloned into the PMX-IRES-GFP and MIG-IRES-mCherry retroviral vectors, respectively. PARP (KU58948), ATM (Ku55933), and DNA-PK (NU7026) inhibitors were obtained from Astra Zeneca and ATRi has recently been described (Toledo et al., 2011).

Flow Cytometry, Metaphase Analysis, and Telomere FISH

For FACs analysis, splenic B cells were stained with fluorochrome-conjugated anti-B220, anti-igG1, and anti-igE antibodies (PharMingen) as described (Wesemann et al., 2011). Carboxyfluorescein succinimidyl ester (CFSE) labeling was performed to track cell division. Samples were acquired on a FACSCalibur (Becton Dickinson), and cell sorting was preformed on a FACSAria (Becton Dickinson). Cells were harvested for metaphase analysis as described (Callén et al., 2007a). The murine TRF2 shRNA-targeting construct and MEF retroviral infection have been described (Rai et al., 2010). Telomere-induced foci were visualized by hybridization with anti-mouse γ-H2AX antibody (Upstate Biotechnology) together with PNA probe (Applied Biosystems). Phosphorylated Kap-1 was detected by flow cytometry after intracellular staining using the BD Cytofix/Cytoperm kit (BD Biosciences).

DNA Damage, Laser Microirradiation, Immunoprecipitation, and RNA-Sequencing

Cells were treated with different DNA damaging agents (IR, CPT, CisPt, and PARPi), and colony survival was assessed after 14 days, or metaphase analysis was performed 24 hr after treatment. For immunofluorescent staining, cells were irradiated with indicated doses of ionizing radiation, allowed to recover, and then fixed and processed as described (Celeste et al., 2003). For microirradiation, cells were presensitized in DMEM media containing 0.1 µg/ml of Hoechst 33342 for 60 min before replacing with phenol red free media containing 5 mM HEPES, and then irradiated with the 364 nm laser line on a LSM510 confocal microscope (Zeiss) equipped with a heated stage. Cells were allowed to recover for 15 min prior to processing for immunofluorescence. Analysis of RPA foci was performed using an Opera High-Content Screening system as described (López-Contreras et al., 2012). Primary antibodies for immunofluorescence were rabbit anti-53BP1 (Novus), mouse anti-γ-H2AX (Upstate Biotechnology), mouse or rabbit anti-FLAG-M2 (Sigma), mouse anti-AIM1 (Becton Dickinson), mouse anti-GFP (Roche), rabbit anti-RAD51 (Santa Cruz), rat anti-RPA (Cell Signaling), rabbit anti-PTIP (Cho et al., 2009), and rabbit anti-RIF1 (Di Virgilio et al., 2013). DNA was counterstained with DAPI. For immunoprecipitation, primary 53BP1^{-/-} B cells were infected with retroviral constructs. Ninety-six hours postactivation, cells were irradiated (10 Gy), left to recover for 45 min, and collected by centrifugation. Cells were lysed, sonicated, and cell lysates were incubated with magnetic beads (M-270 epoxy beads, Invitrogen) conjugated with anti-Flag M2 antibody (Di Virgilio et al., 2013). 53BP1-associated proteins were eluted by incubation in NuPAGE LDS sample buffer (Invitrogen) supplemented with 45 mM DTT for 10 min at 72°C. For RNA sequencing, reads from each cDNA library were mapped onto the Build 37 assembly of the National Center for Biotechnology Information mouse genome data (July 2007; NCBI37/mm9) using TopHat. Bioconductor (Gentleman et al., 2004) was used to calculate the RPKM (reads per kilobase exon model per million mapped reads) of the RefSeq annotated genes.

SUPPLEMENTAL INFORMATION

Supplemental Information includes seven figures and can be found with this article online at <http://dx.doi.org/10.1016/j.cell.2013.05.023>.

ACKNOWLEDGMENTS

We thank all members of the A. Nussenzweig lab and Davide Robbiani for discussions; Titia de Lange for RIF1f/f mice; Susan Sharroo for flow cytometry; and Sandy Chang for the TRF2 shRNA construct. M.C.N., F.W.A and O.F.-C. are HHMI investigators. D.R.W. was supported by NIH grants AI89972, the American Association of Allergy Asthma and Immunology and CSL Behring, and a Career Award for Medical Scientists (Burroughs Wellcome Fund). This work was supported by the Intramural Research Program of the

NIH, the National Cancer Institute, and the Center for Cancer Research, and by a Department of Defense grant to A.N. (BC102335).

Received: March 20, 2013

Revised: April 9, 2013

Accepted: May 10, 2013

Published: May 30, 2013

REFERENCES

- Barlow, J.H., Faryabi, R.B., Callén, E., Wong, N., Malhowski, A., Chen, H.T., Gutierrez-Cruz, G., Sun, H.W., McKinnon, P., Wright, G., et al. (2013). Identification of early replicating fragile sites that contribute to genome instability. *Cell* 152, 620–632.
- Bhattacharyya, A., Ear, U.S., Koller, B.H., Weichselbaum, R.R., and Bishop, D.K. (2000). The breast cancer susceptibility gene BRCA1 is required for sub-nuclear assembly of Rad51 and survival following treatment with the DNA cross-linking agent cisplatin. *J. Biol. Chem.* 275, 23899–23903.
- Boboila, C., Jankovic, M., Yan, C.T., Wang, J.H., Wesemann, D.R., Zhang, T., Fazell, A., Feldman, L., Nussenzweig, A., Nussenzweig, M., and Alt, F.W. (2010). Alternative end-joining catalyzes robust IgH locus deletions and translocations in the combined absence of ligase 4 and Ku70. *Proc. Natl. Acad. Sci. USA* 107, 3034–3039.
- Bothmer, A., Robbiani, D.F., Feldhahn, N., Gazumyan, A., Nussenzweig, A., and Nussenzweig, M.C. (2010). 53BP1 regulates DNA resection and the choice between classical and alternative end joining during class switch recombination. *J. Exp. Med.* 207, 855–865.
- Bothmer, A., Robbiani, D.F., Di Virgilio, M., Bunting, S.F., Klein, I.A., Feldhahn, N., Barlow, J., Chen, H.T., Bosque, D., Callén, E., et al. (2011). Regulation of DNA end joining, resection, and immunoglobulin class switch recombination by 53BP1. *Mol. Cell* 42, 319–329.
- Bouwman, P., Aly, A., Escandell, J.M., Pieterse, M., Bartkova, J., van der Gulden, H., Hiddingh, S., Thanasoula, M., Kulkarni, A., Yang, Q., et al. (2010). 53BP1 loss rescues BRCA1 deficiency and is associated with triple-negative and BRCA-mutated breast cancers. *Nat. Struct. Mol. Biol.* 17, 688–695.
- Bowman-Colin, C., Xia, B., Bunting, S., Klijn, C., Drost, R., Bouwman, P., Fine-man, L., Chen, X., Culhane, A.C., Cai, H., et al. (2013). Palb2 synergizes with Trp53 to suppress mammary tumor formation in a model of inherited breast cancer. *Proc. Natl. Acad. Sci. USA*. Published online May 8, 2013. <http://dx.doi.org/10.1073/pnas.1305362110>.
- Bryant, H.E., Schultz, N., Thomas, H.D., Parker, K.M., Flower, D., Lopez, E., Kyle, S., Meuth, M., Curtin, N.J., and Helleday, T. (2005). Specific killing of BRCA2-deficient tumours with inhibitors of poly(ADP-ribose) polymerase. *Nature* 434, 913–917.
- Bunting, S.F., Callén, E., Wong, N., Chen, H.T., Polato, F., Gunn, A., Bothmer, A., Feldhahn, N., Fernandez-Capetillo, O., Cao, L., et al. (2010). 53BP1 inhibits homologous recombination in Brca1-deficient cells by blocking resection of DNA breaks. *Cell* 141, 243–254.
- Bunting, S.F., Callén, E., Kozak, M.L., Kim, J.M., Wong, N., López-Contreras, A.J., Ludwig, T., Baer, R., Faryabi, R.B., Malhowski, A., et al. (2012). BRCA1 functions independently of homologous recombination in DNA interstrand crosslink repair. *Mol. Cell* 46, 125–135.
- Buonomo, S.B., Wu, Y., Ferguson, D., and de Lange, T. (2009). Mammalian Rif1 contributes to replication stress survival and homology-directed repair. *J. Cell Biol.* 187, 385–398.
- Callén, E., Jankovic, M., Difilippantonio, S., Daniel, J.A., Chen, H.T., Celeste, A., Pellegrini, M., McBride, K., Wangsa, D., Bredemeyer, A.L., et al. (2007a). ATM prevents the persistence and propagation of chromosome breaks in lymphocytes. *Cell* 130, 63–75.
- Callén, E., Nussenzweig, M.C., and Nussenzweig, A. (2007b). Breaking down cell cycle checkpoints and DNA repair during antigen receptor gene assembly. *Oncogene* 26, 7759–7764.

- Callen, E., Faryabi, R.B., Luckey, M., Hao, B., Daniel, J.A., Yang, W., Sun, H.W., Dressler, G., Peng, W., Chi, H., et al. (2012). The DNA damage- and transcription-associated protein paxip1 controls thymocyte development and emigration. *Immunity* 37, 971–985.
- Cao, L., Xu, X., Bunting, S.F., Liu, J., Wang, R.H., Cao, L.L., Wu, J.J., Peng, T.N., Chen, J., Nussenzweig, A., et al. (2009). A selective requirement for 53BP1 in the biological response to genomic instability induced by Brca1 deficiency. *Mol. Cell* 35, 534–541.
- Celeste, A., Fernandez-Capetillo, O., Kruhlak, M.J., Pilch, D.R., Staudt, D.W., Lee, A., Bonner, R.F., Bonner, W.M., and Nussenzweig, A. (2003). Histone H2AX phosphorylation is dispensable for the initial recognition of DNA breaks. *Nat. Cell Biol.* 5, 675–679.
- Celli, G.B., Denchi, E.L., and de Lange, T. (2006). Ku70 stimulates fusion of dysfunctional telomeres yet protects chromosome ends from homologous recombination. *Nat. Cell Biol.* 8, 885–890.
- Chapman, J.R., Barral, P., Vannier, J.B., Borel, V., Steger, M., Tomas-Loba, A., Sartori, A.A., Adams, I.R., Batista, F.D., and Boulton, S.J. (2013). RIF1 is essential for 53BP1-dependent nonhomologous end joining and suppression of DNA double-strand break resection. *Mol. Cell* 49, 858–871.
- Cho, Y.W., Hong, T., Hong, S., Guo, H., Yu, H., Kim, D., Guszczynski, T., Dressler, G.R., Copeland, T.D., Kalkum, M., and Ge, K. (2007). PTIP associates with MLL3- and MLL4-containing histone H3 lysine 4 methyltransferase complex. *J. Biol. Chem.* 282, 20395–20406.
- Cho, Y.W., Hong, S., Jin, Q., Wang, L., Lee, J.E., Gavrilova, O., and Ge, K. (2009). Histone methylation regulator PTIP is required for PPARgamma and C/EBPalpha expression and adipogenesis. *Cell Metab.* 10, 27–39.
- Daniel, J.A., Santos, M.A., Wang, Z., Zang, C., Schwab, K.R., Jankovic, M., Filsuf, D., Chen, H.T., Gazumyan, A., Yamane, A., et al. (2010). PTIP promotes chromatin changes critical for immunoglobulin class switch recombination. *Science* 329, 917–923.
- Di Virgilio, M., Callen, E., Yamane, A., Zhang, W., Jankovic, M., Gitlin, A.D., Feldhahn, N., Resch, W., Oliveira, T.Y., Chait, B.T., et al. (2013). Rif1 prevents resection of DNA breaks and promotes immunoglobulin class switching. *Science* 339, 711–715.
- Difilippantonio, S., Gapud, E., Wong, N., Huang, C.Y., Mahowald, G., Chen, H.T., Kruhlak, M.J., Callen, E., Livak, F., Nussenzweig, M.C., et al. (2008). 53BP1 facilitates long-range DNA end-joining during V(D)J recombination. *Nature* 456, 529–533.
- Dimitrova, N., Chen, Y.C., Spector, D.L., and de Lange, T. (2008). 53BP1 promotes non-homologous end joining of telomeres by increasing chromatin mobility. *Nature* 456, 524–528.
- Escribano-Díaz, C., Orthwein, A., Fradet-Turcotte, A., Xing, M., Young, J.T., Tkáč, J., Cook, M.A., Rosebrock, A.P., Munro, M., Canny, M.D., et al. (2013). A cell cycle-dependent regulatory circuit composed of 53BP1-RIF1 and BRCA1-CtIP controls DNA repair pathway choice. *Mol. Cell* 49, 872–883.
- Farmer, H., McCabe, N., Lord, C.J., Tutt, A.N., Johnson, D.A., Richardson, T.B., Santarosa, M., Dillon, K.J., Hickson, I., Knights, C., et al. (2005). Targeting the DNA repair defect in BRCA mutant cells as a therapeutic strategy. *Nature* 434, 917–921.
- Feng, L., Fong, K.W., Wang, J., Wang, W., and Chen, J. (2013). RIF1 counteracts BRCA1-mediated end resection during DNA repair. *J. Biol. Chem.* 288, 11135–11143.
- Gentleman, R.C., Carey, V.J., Bates, D.M., Bolstad, B., Dettling, M., Dudoit, S., Ellis, B., Gautier, L., Ge, Y., Gentry, J., et al. (2004). Bioconductor: open software development for computational biology and bioinformatics. *Genome Biol.* 5, R80.
- Gong, Z., Cho, Y.W., Kim, J.E., Ge, K., and Chen, J. (2009). Accumulation of Pax2 transactivation domain interaction protein (PTIP) at sites of DNA breaks via RNF8-dependent pathway is required for cell survival after DNA damage. *J. Biol. Chem.* 284, 7284–7293.
- Jaspers, J.E., Kersbergen, A., Boon, U., Sol, W., van Deemter, L., Zander, S.A., Drost, R., Wientjens, E., Ji, J., Aly, A., et al. (2013). Loss of 53BP1 causes PARP inhibitor resistance in Brca1-mutated mouse mammary tumors. *Cancer Discov* 3, 68–81.
- Jowsey, P.A., Doherty, A.J., and Rouse, J. (2004). Human PTIP facilitates ATM-mediated activation of p53 and promotes cellular resistance to ionizing radiation. *J. Biol. Chem.* 279, 55562–55569.
- López-Contreras, A.J., Gutierrez-Martinez, P., Specks, J., Rodrigo-Perez, S., and Fernandez-Capetillo, O. (2012). An extra allele of Chk1 limits oncogene-induced replicative stress and promotes transformation. *J. Exp. Med.* 209, 455–461.
- Lottersberger, F., Bothmer, A., Robbiani, D.F., Nussenzweig, M.C., and de Lange, T. (2013). Role of 53BP1 oligomerization in regulating double-strand break repair. *Proceedings of the National Academy of Sciences of the United States of America*.
- Manke, I.A., Lowery, D.M., Nguyen, A., and Yaffe, M.B. (2003). BRCT repeats as phosphopeptide-binding modules involved in protein targeting. *Science* 302, 636–639.
- Moynahan, M.E., Chiu, J.W., Koller, B.H., and Jasin, M. (1999). Brca1 controls homology-directed DNA repair. *Mol. Cell* 4, 511–518.
- Munoz, I.M., Jowsey, P.A., Toth, R., and Rouse, J. (2007). Phospho-epitope binding by the BRCT domains of hPTIP controls multiple aspects of the cellular response to DNA damage. *Nucleic Acids Res.* 35, 5312–5322.
- Patel, S.R., Kim, D., Levitan, I., and Dressler, G.R. (2007). The BRCT-domain containing protein PTIP links PAX2 to a histone H3, lysine 4 methyltransferase complex. *Dev. Cell* 13, 580–592.
- Rai, R., Zheng, H., He, H., Luo, Y., Multani, A., Carpenter, P.B., and Chang, S. (2010). The function of classical and alternative non-homologous end-joining pathways in the fusion of dysfunctional telomeres. *EMBO J.* 29, 2598–2610.
- Reina-San-Martin, B., Chen, J., Nussenzweig, A., and Nussenzweig, M.C. (2007). Enhanced intra-switch region recombination during immunoglobulin class switch recombination in 53BP1-/- B cells. *Eur. J. Immunol.* 37, 235–239.
- Schwab, K.R., Patel, S.R., and Dressler, G.R. (2011). Role of PTIP in class switch recombination and long-range chromatin interactions at the immunoglobulin heavy chain locus. *Mol. Cell. Biol.* 31, 1503–1511.
- Scully, R., Chen, J., Plug, A., Xiao, Y., Weaver, D., Feunteun, J., Ashley, T., and Livingston, D.M. (1997). Association of BRCA1 with Rad51 in mitotic and meiotic cells. *Cell* 88, 265–275.
- Sfeir, A., and de Lange, T. (2012). Removal of shelterin reveals the telomere end-protection problem. *Science* 336, 593–597.
- Silverman, J., Takai, H., Buonomo, S.B., Eisenhaber, F., and de Lange, T. (2004). Human Rif1, ortholog of a yeast telomeric protein, is regulated by ATM and 53BP1 and functions in the S-phase checkpoint. *Genes Dev.* 18, 2108–2119.
- Sonoda, E., Hochegger, H., Saberi, A., Taniguchi, Y., and Takeda, S. (2006). Differential usage of non-homologous end-joining and homologous recombination in double strand break repair. *DNA Repair (Amst.)* 5, 1021–1029.
- Symington, L.S., and Gautier, J. (2011). Double-strand break end resection and repair pathway choice. *Annu. Rev. Genet.* 45, 247–271.
- Toledo, L.I., Murga, M., Zur, R., Soria, R., Rodriguez, A., Martinez, S., Oyarzabal, J., Pastor, J., Bischoff, J.R., and Fernandez-Capetillo, O. (2011). A cell-based screen identifies ATR inhibitors with synthetic lethal properties for cancer-associated mutations. *Nat. Struct. Mol. Biol.* 18, 721–727.
- Wang, X., Takenaka, K., and Takeda, S. (2010). PTIP promotes DNA double-strand break repair through homologous recombination. *Genes Cells*. Published online January 19, 2013. <http://dx.doi.org/10.1111/j.1365-2443.2009.01379.x>.
- Ward, I.M., Reina-San-Martin, B., Olaru, A., Minn, K., Tamada, K., Lau, J.S., Cascalho, M., Chen, L., Nussenzweig, A., Livak, F., et al. (2004). 53BP1 is required for class switch recombination. *J. Cell Biol.* 165, 459–464.

- Ward, I., Kim, J.E., Minn, K., Chini, C.C., Mer, G., and Chen, J. (2006). The tandem BRCT domain of 53BP1 is not required for its repair function. *J. Biol. Chem.* **281**, 38472–38477.
- Wesemann, D.R., Magee, J.M., Boboila, C., Calado, D.P., Gallagher, M.P., Portuguese, A.J., Manis, J.P., Zhou, X., Recher, M., Rajewsky, K., et al. (2011). Immature B cells preferentially switch to IgE with increased direct S μ to S ϵ recombination. *J. Exp. Med.* **208**, 2733–2746.
- Yamane, A., Robbiani, D.F., Resch, W., Bothmer, A., Nakahashi, H., Oliveira, T., Rommel, P.C., Brown, E.J., Nussenzweig, A., Nussenzweig, M.C., and Casellas, R. (2013). RPA accumulation during class switch recombination represents 5'-3' DNA-end resection during the S-G2/M phase of the cell cycle. *Cell Rep* **3**, 138–147.
- Yu, X., Chini, C.C., He, M., Mer, G., and Chen, J. (2003). The BRCT domain is a phospho-protein binding domain. *Science* **302**, 639–642.
- Zimmermann, M., Lottersberger, F., Buonomo, S.B., Sfeir, A., and de Lange, T. (2013). 53BP1 regulates DSB repair using Rif1 to control 5' end resection. *Science* **339**, 700–704.

Supplemental Information

Cell

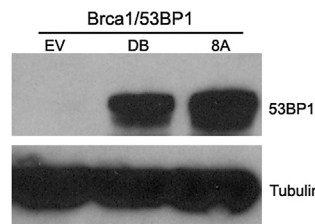
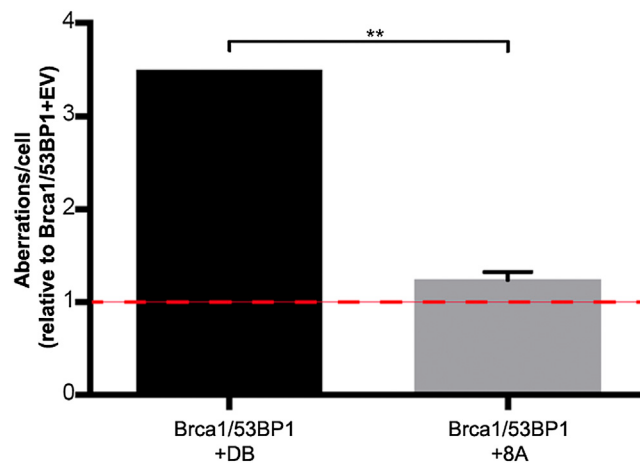


Figure S1. Genome Instability in *BRCA1*^{-/-}*53BP1*^{-/-} MEFs, Related to Figure 1

BRCA1^{-/-}*53BP1*^{-/-} MEFs were reconstituted with empty vector (EV), 53BP1^{DB}, and 53BP1^{8A} retroviruses. Top: Normalized genome instability in metaphase spreads after PARPi treatment (24 hr) measured in two independent experiments, and expressed relative to *BRCA1*^{-/-}*53BP1*^{-/-} MEFs reconstituted with EV. Dashed line represents normalized genomic instability in *BRCA1*^{-/-}*53BP1*^{-/-} +EV (**:p < 0.01, one-tailed unpaired t test). Error bars represent SEM. Bottom: western blot analysis of 53BP1 and tubulin in reconstituted cell lines.

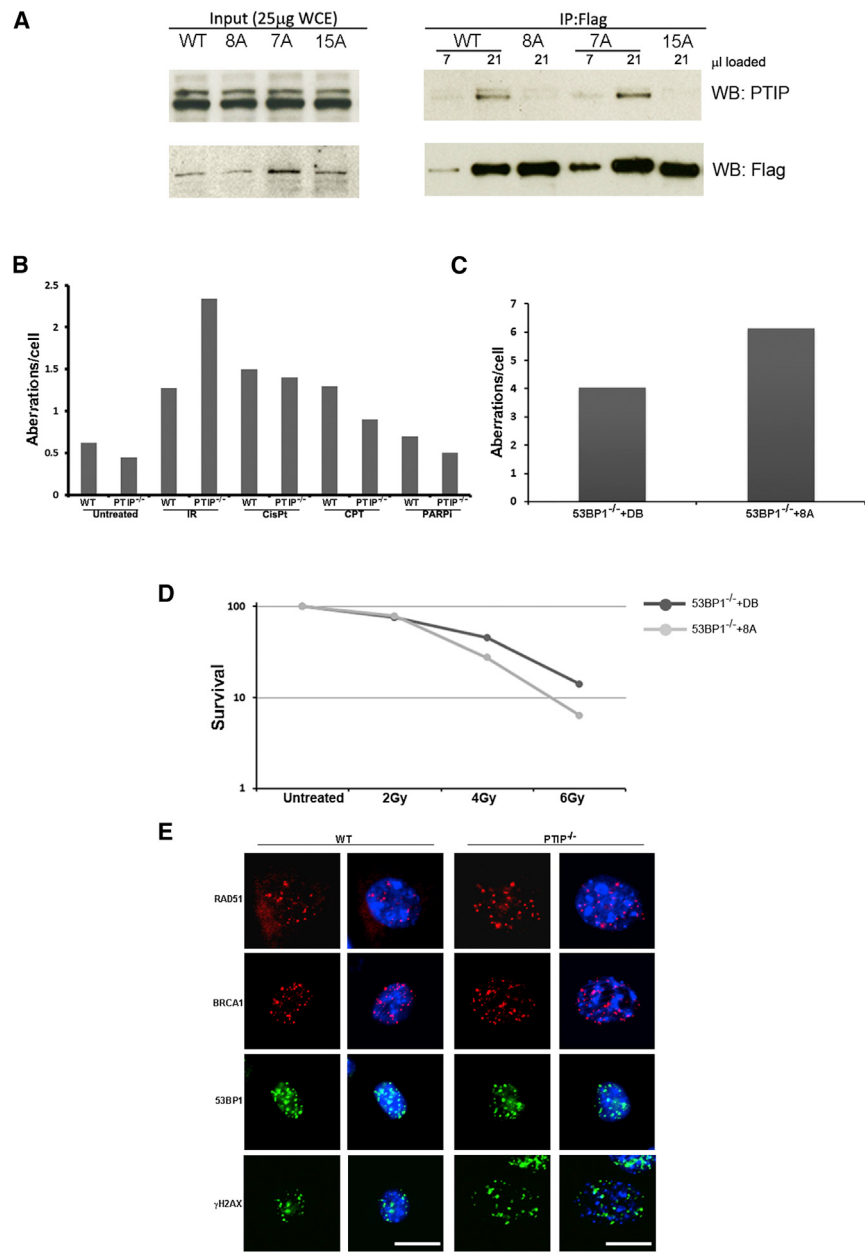


Figure S2. Response of 53BP1- and PTIP- Mutant Cells to IR, Related to Figure 2

(A) Phosphorylation of S/TQ sites in 7A domain is dispensable for PTIP interaction with 53BP1. Western blot analysis of anti-Flag immunoprecipitates from irradiated (10 Gy, 45 min recovery) 53BP1^{-/-} B cells infected with the indicated retroviral constructs. All IP reactions were eluted in 30 µl of PAGE sample loading buffer. 3x-fold IP sample dilutions (7 µl and 21 µl, respectively) were loaded for wild-type and 7A mutant 53BP1 to show that mutagenesis of S/TQ sites in 7A domain does not impair PTIP interaction with 53BP1.

(B) WT and PTIP^{-/-} MEFs were either untreated or treated with irradiation (IR, 2 Gy), cisplatin (CisPt, 0.5 µM), camptothecin (CPT, 10 nM) or PARP inhibitor (PARPi, 1 µM) and chromosomal aberrations were quantified in at least 50 metaphase spreads for each genotype and each treatment. An independent measurement is shown in Figure 2B.

(C) IR response of 53BP1^{-/-} MEFs reconstituted with 53BP1^{DB} and 53BP1^{8A}. Cells were irradiated (2 Gy), and metaphase spreads were analyzed for chromosomal damage after 24 hr. Results are representative of two independently performed experiments.

(D) 53BP1^{DB} and 53BP1^{8A} MEFs were treated with indicated doses of IR and colony formation was assessed.

(E) Immunostaining for RAD51 (red), BRCA1 (red), 53BP1 (green) and γ-H2AX (green) in WT and PTIP^{-/-} MEFs. Cells were treated with 10 Gy and harvested at 2hrs post-IR for 53BP1 and γ-H2AX, and 4hrs for BRCA1 and RAD51. DAPI counterstain is shown in blue. Scale bar, 10 µm.

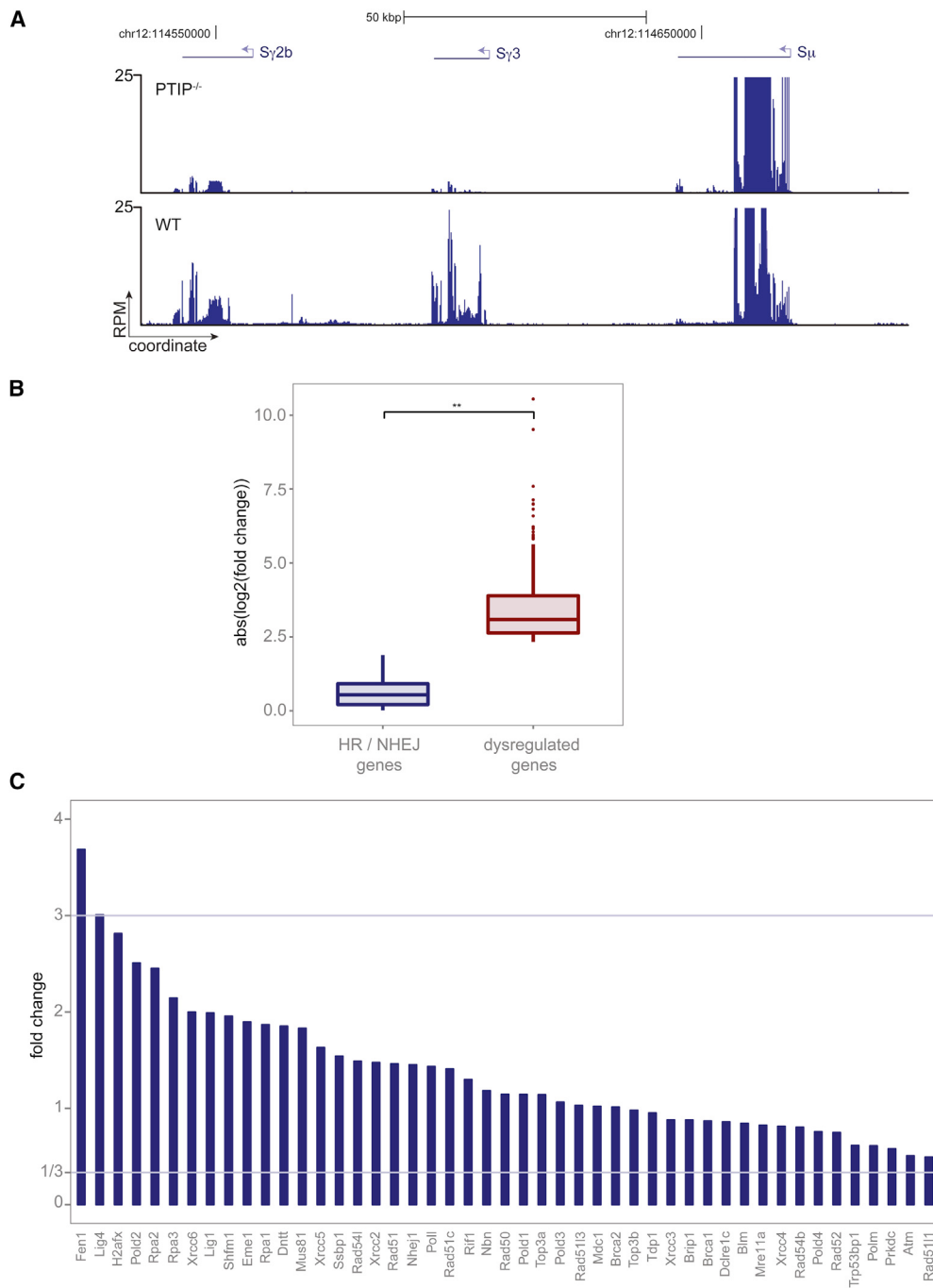


Figure S3. Transcription of HR and NHEJ Genes Is Independent of PTIP, Related to Figure 5

(A) Transcription of S γ 3/S γ 2b is PTIP dependent. RNA-Seq read histograms at the S μ , S γ 2b, and S γ 3 of IgH switch regions in WT and PTIP^{-/-} B cells activated by LPS and α -IgD-dextran are shown. The x axis represents the linear sequence of genomic DNA, and the y axis represents reads per million aligned reads (RPM). The genomic scale in kilo-base pairs (kbp) is indicated above the tracks.

(B) Transcription of genes in HR and NHEJ pathways are PTIP independent. Box-plots show the quantiles of absolute logarithmic gene expression fold change at dysregulated genes versus genes in HR and/or NHEJ pathways (**: p value < 1 × 10⁻⁷; Mann-Whitney test).

(C) Genes in DSB repair pathways are not deregulated by PTIP. Bar graphs show the fold change in gene transcription level in PTIP^{-/-} cells relative to WT cells. Horizontal lines demarcate the 3-fold increase and decrease levels.

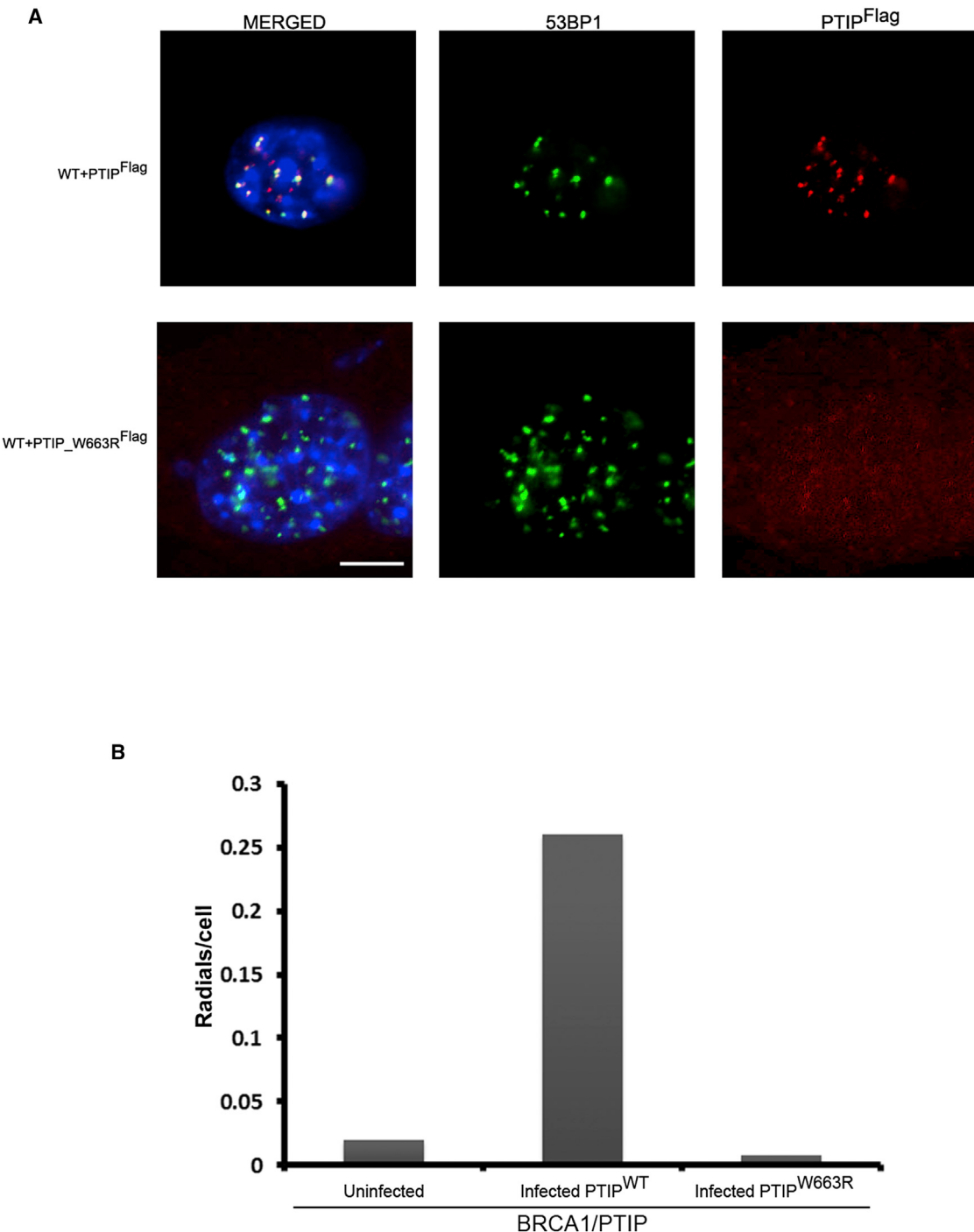


Figure S4. The W663R Mutation in PTIP Abrogates DSB Recruitment and PARPi Sensitivity of BRCA1-Deficient Cells, Related to Figure 5
 (A) WT MEFs expressing FLAG-tagged PTIP^{WT} and PTIP^{W663R} were irradiated with 10 Gy IR. 53BP1 (green) and PTIP (red) foci were assessed using anti-53BP1 and -FLAG antibodies, respectively.

(B) *BRCA1*^{-/-}PTIP^{-/-} B cells were reconstituted with PTIP^{WT} or PTIP^{W663R} retroviruses and treated with PARPi. Cells were sorted (GFP^{positive} = infected and GFP^{negative} = uninfected) and metaphases were analyzed for radial chromosomes ($n = 50$ metaphases analyzed in each case). Data from an independent experiment is shown in Figure 5F.

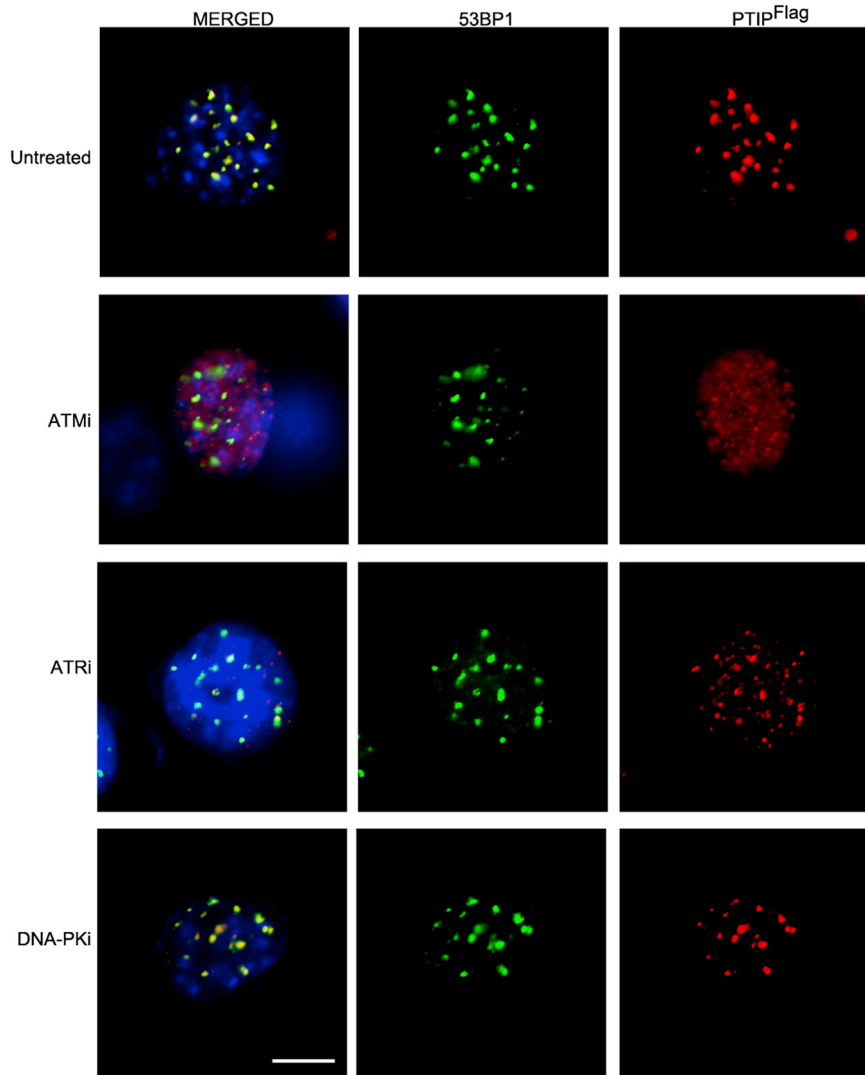


Figure S5. ATM Is the Primary Kinase Responsible for PTIP Recruitment to IRIF, Related to Figure 6

WT MEFs expressing PTIP-FLAG were pretreated with inhibitors of ATM, ATR and DNA-PKcs, cells were irradiated with 10 Gy, and PTIP (red) and 53BP1 (green) IRIF were assessed 4 hr later. Representative cells are shown. Scale bar, 10 μ m.

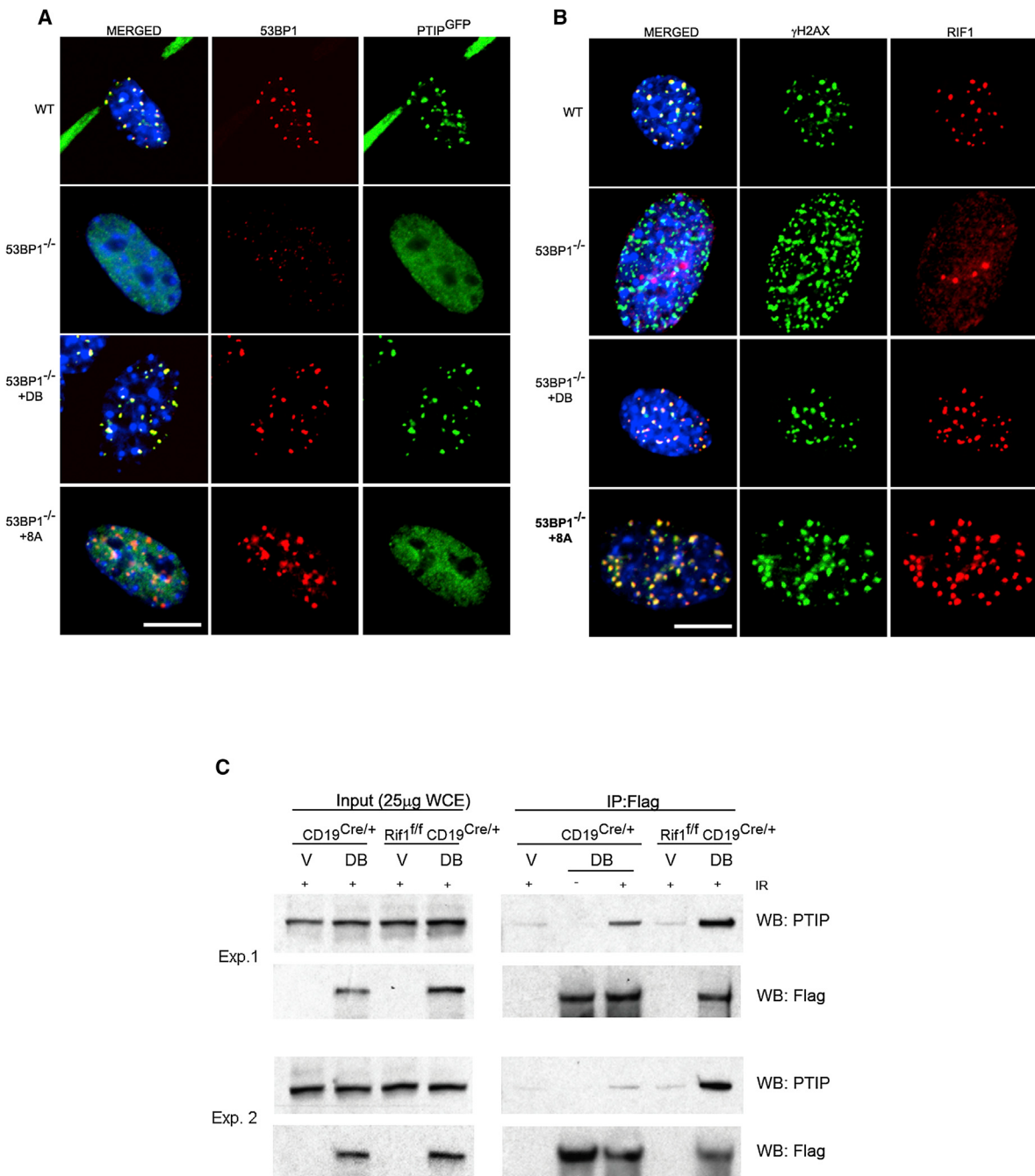


Figure S6. PTIP Association with 53BP1 at DSBs Is Dependent on the Eight Most N-Terminal S/TQ Phosphorylation Sites and Is Limited by RIF1, Related to Figure 7

(A) MEFs (WT, 53BP1^{-/-}, and 53BP1^{-/-} reconstituted with 53BP1^{DB} or 53BP1^{8A}) were infected with GFP-PTIP, irradiated (10 Gy, 4 hr recovery) and then stained with anti-53BP1 (red) and anti-GFP antibodies. Scale bar, 10 μ m.

(B) Same cell lines as in (A) were costained with γ -H2AX (green) and RIF1 (red). DAPI counterstain (blue) is shown. Scale bar, 10 μ m.

(C) RIF1 limits the amount of PTIP binding to 53BP1. Western blot analysis of anti-Flag immunoprecipitates from B cells of the indicated genotypes infected with empty vector (v) or Flag-tagged 53BP1^{DB} (DB). Cells were either left untreated or irradiated (10 Gy, 45 min recovery). Two independent experiments are shown.

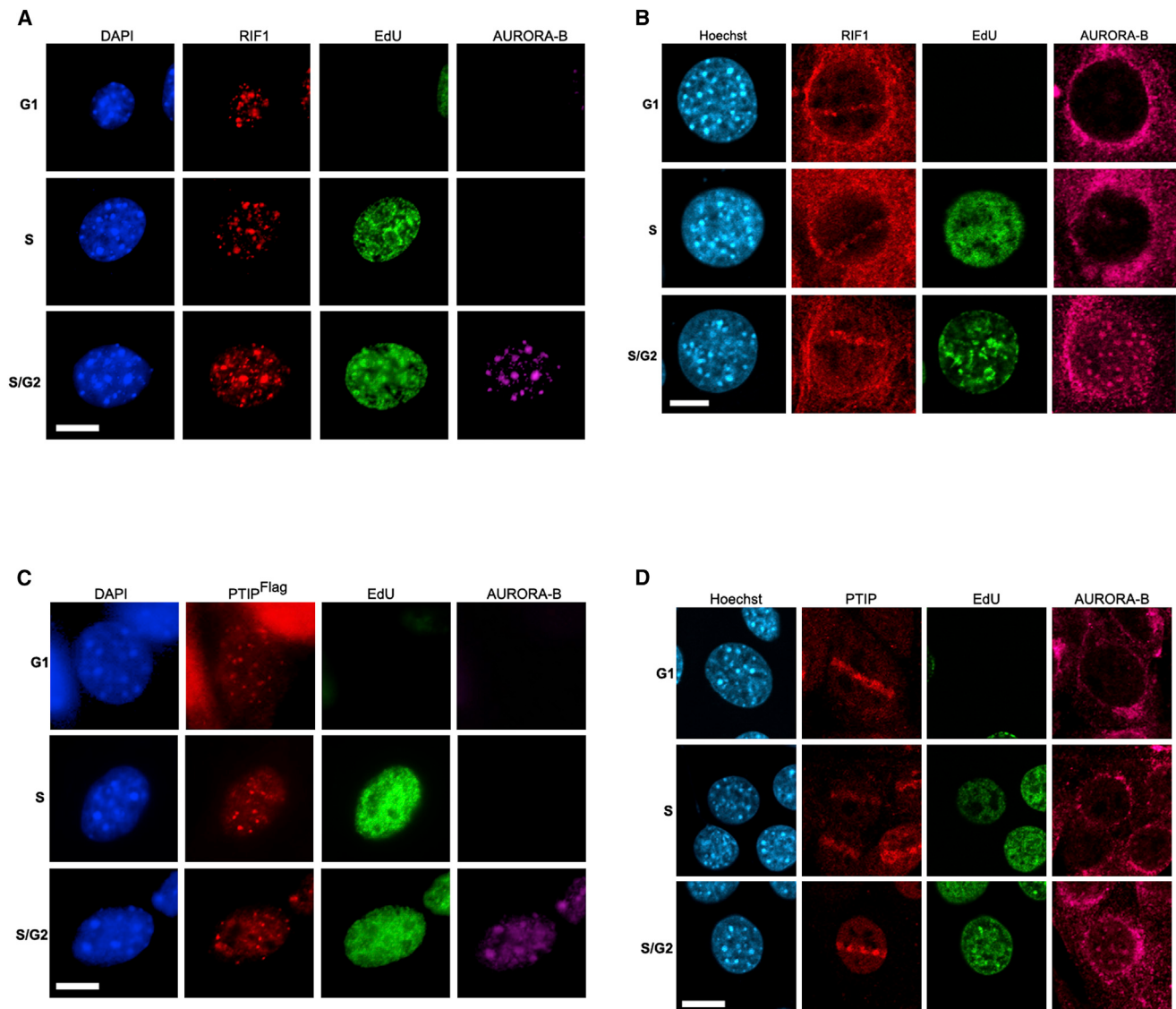


Figure S7. RIF1 and PTIP Are Recruited to DSBs in G1 and S/G2 Phases of the Cell Cycle, Related to Figure 7

WT MEFs were pulsed with 20 μ M EdU, irradiated with 10 Gy (A) or exposed to laser microirradiation (B), incubated with Alexafluor 488 conjugated Click-It EdU labeling mixture (Invitrogen), and immunolabeled with anti-AIM1 (Aurora B) (1:100 dilution) and anti-RIF1 (1:1,000 dilution) antibodies. (C and D) WT^{PTIP-FLAG} MEFs were treated as above and stained with an anti-FLAG antibody (1:200 dilution) (C) or an anti-PTIP antibody (1:1,000 dilution) (D). Representative images are shown. Scale bars, 10 μ m.